Version of Record: https://www.sciencedirect.com/science/article/pii/S0025322719301781
Manuscript_0898f9e3e9606b04d2fa54f8bab4a783

Flood deposition and storm removal of sediments in front of a deltaic wave-influenced river mouth

Authors:

Florin Zăinescu

(a) University of Bucharest, Faculty of Geography, Bulevardul Nicolae Bălcescu 1, București 010041, Romania.

(b) Aix Marseille University, CNRS, IRD, INRA, Coll France, CEREGE, Aix-en-Provence, France

florinzainescu@yahoo.com

Alfred Vespremeanu-Stroe

University of Bucharest, Faculty of Geography, Bulevardul Nicolae Bălcescu 1, București 010041, Romania.

fredi@geo.unibuc.ro

Edward Anthony

(a) Aix Marseille University, CNRS, IRD, INRA, Coll France, CEREGE, Aix-en-Provence, France

(b) CNRS, UG, IFREMER, LEEISA USR 3456, Centre de recherche de Montabo, Cayenne, Guyane française

anthony@cerege.fr

Florin Tătui

University of Bucharest, Faculty of Geography, Bulevardul Nicolae Bălcescu 1, București 010041, Romania.

florin.tatui@geo.unibuc.ro

Luminita Preoteasa

University of Bucharest, Faculty of Geography, Bulevardul Nicolae Bălcescu 1, București 010041, Romania.

luminita.preoteasa@geo.unibuc.ro

Răzvan Mateescu

National Institute for Marine Research and Development "Grigore Antipa", 300 Mamaia Blvd., RO-900581, Constanta, Romania

razvan_doru@yahoo.com

Corresponding author: Florin Zăinescu

Flood deposition and storm removal of sediments in front of a deltaic wave-influenced river mouth

Abstract

Floods and storms are common phenomena at river mouths with some degree of wave influence. They can have a considerable impact on river-mouth sedimentation and morphological change, although studies elucidating this relationship are relatively rare. The present paper analyzes annual bathymetric changes based on surveys at the mouth of the Sfântu Gheorghe branch of the Danube river delta between 2004 and 2018, and relates bed changes with measured river freshwater and solid discharges, and wave height data. We found a strong inter-annual variability of morphological volume change which ranged from 5.23×10^6 m^3 deposited during the extreme flood of 2006 (maximum discharge of ~4000 m^3/s), to -6.88×10^6 m^3 removed during the stormy year of 2012 (wave heights > 6 m). The sediment budget of the river-mouth area is modulated by the inter-annual variability of storms and floods, and can be estimated by the newly proposed Flood/Storm index based on river water or sediment discharge and wave height proxies (R^2=0.84). A selection of discharge and wave thresholds were simulated with Mike 21/3 by DHI (Danish Hydraulic Institute), a coupled hydrodynamic and wave model to characterize circulation and the applied bed shear stresses at this complex river-mouth sedimentary system. The model simulates 3D jet and plume hydrodynamics during floods, and the longshore current and wave dissipation during storms. Finally, field data are integrated with the Mike 21/3 model results to derive a conceptual hydro-morphodynamic model of an asymmetric wave influenced river-mouth bar during the two antagonistic phases of flood-driven

and storm-driven dynamics. During floods, the importance of current circulation and counter-plume currents in trapping sediments in a seaward-thinning depositional wedge is discussed. During storms, the sediment deposited during floods is removed by the high bed shear stresses generated by waves and currents.

Keywords: Wave-river-influenced delta; River mouth; Storms; Floods; Mouth bar; Mike 3; Delta processes

1. INTRODUCTION

Modern deltas are environmental archives of fast evolving coastal configurations, spanning, for many deltas the last 8 ka (Stanley and Warne, 1994; Hori et al., 2004; Tamura et al., 2009; Vespremeanu-Stroe et al., 2017), and involving shifting depocentres associated with river mouths and their interaction with the dispersive oceanographic forces represented by waves, tides and currents (Anthony, 2015a). Delta construction is achieved by the trapping of a large part of sediment supplied by river mouths and longshore currents close to the shoreline in shallow waters. Nevertheless, river mouths worldwide show a wide spectrum of depositional and erosional processes. Large deltas with high sediment supply and comparatively low dispersive agents may trap close to 80% of the sediment delivered by rivers close to their river mouths, forming subaqueous delta fronts (e.g. Milliman et al., 1984; Wright, 1985; Bornhold et al., 1986; Sabatier et al., 2006; Ta et al., 2002; van Maren and Hoekstra, 2005; Correggiari et al., 2005; Maillet et al., 2006; Harris et al., 2008; Xue et al., 2010; Szczuciński et al., 2013, Preoteasa et al., 2016). On the contrary, river mouths encountering basins with efficient sediment-dispersing

47 agents usually fail to build protruding deltas (Boyd et al., 1992; Walsh and Nittrouer 2009; Ma et
48 al., 2008), although coastal accumulation of Holocene sediment can still be significant.
49 Nevertheless, for both low and high dispersal systems, the initial flood sediment deposition zone
50 near the river mouths often differs spatially from the final depocentre (e.g., Wright and Nittrouer,
51 1995; Allison et al., 2000; Carlin and Dellapenna, 2014; Marion et al., 2010). The distance to the
52 nearest maximum shelf depocentre (i.e. zone of highest sedimentation over the medium- to long-
53 term) is clearly dependent on significant wave height (H_s) and tidal range. Given sufficient
54 sediment discharge and shelf width, depocentres are found close to river mouths, <10 m depth
55 for H_s <1 m and tidal range <2 m (Walsh and Nittrouer, 2009); whereas for increasing H_s and
56 tidal range, sediment can be deposited far offshore (Walsh and Nittrouer, 2009). Rivers such as
57 the Danube or the Po have built a subaqueous delta front (e.g., Correggiari et al., 2005; Tătui and
58 Vespremeanu-Stroe, 2017) with a sigmoid deposition shape characteristic of relatively low
59 sediment dispersal. Nevertheless, a mid-shelf prodelta clinoform built from fine sediments, offset
60 well alongshore from the river mouths, may be still present (Corregiari et al., 2005;
61 Constantinescu and Giosan, 2017). Rivers draining into narrow shelves associated with active
62 margins and small drainage basins (e.g. Columbia, Eel) are more likely to have their sediment
63 load transported to the deeper shelf, forming mid-shelf mud deposits (Harris et al., 2005), or to
64 the continental slope and down the submarine canyons (Savoye et al., 2009; Warrick 2014).
65 Mechanisms such as wave resuspension and wave- and current-assisted gravity flows become
66 important in carrying sediment offshore and alongshore (Traykovski et al., 2000; Friedrichs and
67 Scully 2007; Harris et al., 2005; Ma et al., 2008). Such ‘wave-supported’ gravity flows,
68 considered as a class of turbidity currents (Wright and Friedrichs, 2006), may be significantly

enhanced by storm activity (Dail et al., 2007). Long-term deposition from these processes may lead to clinoform development, as off the Po (Friedrichs and Scully, 2007).

The Sfântu Gheorghe (Sf. Gheorghe) is one of the world's better-studied deltaic lobes, and an archetype for asymmetric wave-influenced mouths (Bhattacharya and Giosan 2003; Preoteasa et al., 2016). Many authors have described different relevant aspects of the Sf. Gheorghe coastal system: coastal circulation and plume dynamics in the river-mouth area (Bondar et al., 1991; Dinu et al., 2013; Constantin et al., 2017), long-term coastal and shoreface evolution (Vespremeanu, 1983; Preoteasa et al., 2017; Tătui and Vespremeanu-Stroe, 2017), decadal shoreline change linked with storminess (Vespremeanu-Stroe et al., 2007), and longshore transport on the adjacent coasts (Giosan et al., 1999, Vespremeanu-Stroe, 2004; Dan et al., 2009). Clearly, a better understanding of the nature of the sediment dispersal system prevailing at the mouth of this branch and the sediment accumulation and redistribution processes that drive the morphodynamics of the river-mouth area are needed in order to obtain a coherent image of various aspects of the short- to long-term geomorphic evolution of the mouth of the Sf. Gheorghe. The results and their discussion may also be relevant to other wave-influenced delta distributary mouths where significant deposition and resuspension occur close inshore in response to flood and storm-wave alternation.

The objective of this paper is twofold:

i) establish a relationship between, on the one hand, observed morphological change at the mouth, expressed as volume change (ΔV), and, on the other, water discharge (Q), sediment discharge (Q_s), and significant wave height (H_s);

ii) characterize the hydrodynamics and wave processes involved in morphological change.

We address these goals by combining measured data and numerical modelling. To this end, we used data from yearly bathymetric measurements (2004-2018) at the Sf. Gheorghe river-mouth area and applied numerical modelling (Mike 21/3) for wave and hydrodynamic simulations. Measured morphological change was correlated with the results of numerical modelling to derive a conceptual morpho-hydrodynamic model during floods and storms for the river mouth. We further propose a simple, index-based approach in order to explain the variability of yearly sediment budget changes at the river mouth.

2. Regional Setting

The Danube River basin (~800,000 km^2) covers a large part of Central and Southeast Europe and drains a significant part of the Alps and much of the Carpathian Mountains (Fig. 1A). It has an average elevation of about 475 m (Stănescu, 1967), a temperate continental climate with a mean annual air temperature of about 10 °C and mean annual precipitation of around 600 mm/y (Malagó et al., 2017). The river has a length of 2860 km, making it the 29th longest in the world and the 2nd in Europe. It discharges into the Black Sea through five main outlets: Oceakov, Bistroe and Stambul (part of the Chilia main branch, in the north), Sulina (central) and Sf. Gheorghe (south) (Fig. 1).

The river's hydrological regime is pluvio-nival with an average discharge (Q) at the delta apex of about 6800 m^3/s (based on 2004-2015 INHGA data). About 5-8% of the discharge is lost

to infiltration and evaporation in the delta plain and outflow through minor outlets into the Black Sea (Bondar et al., 2011; Bondar and Iordache 2016). Discharge exhibits a moderate seasonal contrast. Floods usually occur from March to June, last for several weeks to a few months, and are linked to the stationary behaviour of Rossby waves in the Northern Hemisphere associated with strong synoptic depressions that generate persistent precipitation (Blöschl et al., 2013). The maximum Q in April 2006 was about 16,000 m^3/s, and was the greatest flood in the last 100 years. Current suspended sediment discharge (Qs) averages 640 kg/s (2004-2015 INHGA data), a threefold decrease relative to values prior to the construction of the Iron Gates dams (Preoteasa et al., 2016). The monthly suspended sediment discharge values recorded during the last floods (2005, 2006, 2010, 2013), although extreme from a Q perspective, remained lower than the mean annual Q_s of the 1840-1980 period. Although bedload has been considered as currently unaffected (Bondar et al., 2011), bedload values are not known.

The Danube is a Proximal Accumulation Dominated (PAD) dispersal system (following Walsh and Nittrouer 2009), with most of the solid discharge being deposited close to the river mouths. The Sf. Gheorghe displays a prominent river-mouth bar (*RMB*) that is asymmetric in morphology (Bhattacharya and Giosan, 2003; Preoteasa et al., 2016), with a protruding updrift crest with depths of around 1.5 - 2 m and a deeper channel downdrift (south) with depths of around 3 - 3.5 m (Fig. 2A; Suppl. 1). North of the river mouth, two to three longshore linear sand bars exhibit an offshore migration of 20–50 m yr^{-1} (Tătui et al., 2016) .The sand-mud transition during a survey in 2005 occurred at about 5 – 6 m depth in front of the river mouth (Fig. 2B), whereas a few km alongshore, the transition occurred at about 8 m depth. Generally, sorting follows the same distribution of the D50 grain size presented in Fig. 2B, with moderately to well sorted (0.2 to 1 Φ) sands, whereas silts are poorly sorted (around 2 Φ). Samples in the north and

central river mouth-area show a a positive skewness (0 to 0.5 Φ), indicative of a higher proportion of fine sediments, whereas southern samples are coarse-skewed (0.3 Φ). A selection of shallow cores taken in 2004 in the river-mouth area (Fig. 2B) demonstrates the interbedded nature of the deposits. A core taken on the RMB crest (Gv1) was composed of mixed silt and sand layers, whereas a core positioned slightly inside the RMB crest (Gv4) was predominantly sandy with a few silt layers. Immediately south of the river mouth, core Gv11 showed a predominanly silty layer down to 20 cm depth and sand afterwards, whereas north of the river mouth, Gv20 was mainly sandy with a few silt layers.Flood-storm interaction is not a dominant occurrence at the river mouth, as severe storms generally occur in winter before the flood season (Fig. 3). The mouth of the Sf. Gheorghe is subject to minor tidal influence with a maximum spring tide range of 0.12 m (Bondar and Panin, 2001). Tides thus have a negligible morphologic imprint. The average significant wave height (H_s) is 0.9 m, and, usually, 20-30 storms exceed the wind speed threshold of 10 m/s and a H_s of 1.5 m each year, and just a few, if any, exceed 20 m/s and a H_s of 4 m (Zăinescu et al., 2017). The most severe are due to the passage of well-developed extratropical cyclones. The dominant northeasterly waves approach the Sf. Gheorghe shoreline at an acute angle, generating a net estimated longshore transport (*LST*) of sand-sized material of ~ 1×10^6 m^3/yr (Vespremeanu-Stroe, 2004; Dan et al., 2009).

3. METHODS

3.1 Bathymetric data

We used yearly bathymetric measurements from 2004 to 2018, as part of the morphological monitoring programme conducted by the Sf. Gheorghe Marine and Fluvial Research Station (SCMF) of the University of Bucharest for the area > 1 m depth in front of the river mouth. The data were collected along shore-perpendicular profiles, usually down to depths of -20 m. The 2004-2013 data were acquired with a Garmin GPSMAP298C echo sounder (accuracy ±0.1%), whereas since 2014 acquisitions have been carried out using a Valeport Midas Surveyor single-beam echo sounder (accuracy ±0.02 m). Measurements are vertically corrected for water-elevation variability with levels from the Sfântu Gheorghe gauge station.

Based on these data, we constructed Digital elevation models (DEMs) on a 4 × 4 km maximum grid using Natural Neighbour Interpolation in Golden Software's Surfer with a grid cell dimension of 50 m × 50 m, and with an anisotropy of 0.7 in a North-South direction in order to better represent alongshore features. Some bathymetric surveys such as those of 2004 and 2013 covered a smaller surface. Next, DEMs of Difference (DoDs) were generated by subtracting grids to obtain bathymetric changes, and we ended by calculating the sediment budgets between surveys on overlapping grids for four areas (Fig. 2A): (i) the Danube channel ($Danube_{channel}$); (ii) the river-mouth bar crest region, a dynamic area considered as the zone of strongest morphological change in the immediate vicinity of the river mouth, with maximum depths of around 8 m (RMB_{crest}); (iii) the upper shoreface, from the shoreline to depths of -8 to -10 m (*Nearshore*); (iv) the river-mouth offshore area, extending from the upper shoreface down to -16 m depth corresponding to the lower shoreface and prodelta (*Offshore*). The alongshore limits of the last two are about ± 1.5 km N-S from the mouth. Estimating errors from bathymetries is difficult as sources of uncertainties are multiple and not easily quantifiable (Hare et al., 2011). These include errors induced by roll, pitch, heading and sound speed structure. A tentative

182 estimation of these unaccounted-for errors, for the 8.8 km^2 common surface retained for volume
183 measurements and for a ± 5cm error, yielded a total of ± 0.44 × 10^6 m^3. Errors for measurable
184 sources from the instruments used and DEM construction are low, generally near or under ± 0.1
185 × $10^6 m^3$ (Table S1).
186
187 *3.2 Waves and river discharge*
188
189 We used wave data from ERA-Interim, a state-of-the-art climate reanalysis made
190 available by the European Centre for Medium-Range Weather Forecasts (ECMWF) (Dee et al.,
191 2011). 3-hourly analysis fields are available at a horizontal resolution of 80 km; more
192 information on the ERA-Interim dataset can be found at
193 https://www.ecmwf.int/en/forecasts/datasets/reanalysis-datasets/era-interim.
194 The following parameters were used: significant height of combined wind waves and
195 swell (H_s), mean wave direction (*dir*), and mean wave period (T). We retrieved the wave time
196 series from a grid point located SE of the Sf. Gheorghe mouth at -35 m water depth. We assessed
197 the quality of the ERA-Interim data by comparing them with 6-hourly recorded observations
198 from the Gloria oil platform (~45 m depth; Fig. 1) for the period 1 Jan 1998 – 31 Dec 2007. We
199 obtained a good Pearson coefficient of correlation, R, of 0.86 and a root mean square error
200 (RMSE) of 0.4 m. The average H_s of the ERA-Interim data is 0.82, whereas it is 0.92 for the
201 Gloria data, indicating a slight negative bias for higher H_s.
202 Discharge data comprise daily liquid discharge (Q) and monthly solid discharge (Q_s)
203 reconstructed for the mouth of Sf. Gheorghe. Reliable daily Q and Q_s are measured only at the
204 hydrologic stations upstream of the Danube delta because of the inability to correctly reconstruct

Q based on the water level, which can fluctuate at river mouths due to winds and waves, in addition to river discharge. As such, we derived our daily Q and Q_s data at the Sf. Gheorghe mouth from the Tulcea station (Fig. 1) by applying a correction factor of 0.53, which represents the percentage of Sf. Gheorghe Q at Tulcea Q (53%) (based on INHGA 2004-2015 monthly Q data). This is in agreement with the Delft Hydraulics Report (van Gils et al., 2006), and the ratio remained relatively unchanged between 2004 and 2015. Daily water levels at Tulcea are available for 2004-2018, whereas daily Q only from June 2015 to July 2018. To extrapolate the Q data for the missing period, we applied a rating curve. The Q for Sf. Gheorghe (Q_{sfGhe}) based on level measurements at Tulcea then becomes:

$$Q_{SfGhe} = 0.53\ (1\mathrm{E}-7\mathrm{x}^4 - \ 5\mathrm{E}-5\mathrm{x}^3 + \ 0.0142\mathrm{x}^2 + \ 10.523\mathrm{x} \ + \ 933.92) \qquad (1)$$

where,

x is water level at Tulcea.

We obtained an $R^2 = 0.9987$, using a fourth order polynomial with the aim of maximizing representativeness for higher discharges, and a RMSE of 54.5 m^3/s. There are still four months in 2015 for which, in the absence of daily Q or water levels, we used average monthly values. For 2016-2018, in the absence of monthly Q_s data, we extrapolated from the Q - Q_s relation in 2004-2015 ($R^2 = 0.83$, RMSE 125 kg/s), based on a power law function, given the fact that sediment concentration increases rapidly with flow:

$$Qs = 1E-5Q^{2.0999} \qquad (2)$$

228 Table 1 shows representative percentiles of discharge and wave height, including Q_{75} (the 75th
229 percentile of discharge) and H_{s90} (the 90th percentile of wave height), which were used
230 throughout the paper.
231
232 *3.3 Numerical modelling*
233
234 Mike by DHI is a state-of-the-art numerical model used in coastal studies for simulating
235 hydrodynamic, wave, and sediment transport processes. The package used in this study
236 comprises the following modules: Mike 3 FM (Flow module), Mike 21 SW (Spectral waves)
237 Mike 3 MT (Mud transport), with the capability of running in coupled mode. Mike 3 FM is
238 based on the three-dimensional incompressible Reynolds-averaged Navier–Stokes equations
239 based on the assumptions of Boussinesq and hydrostatic pressure. It consists of continuity,
240 momentum, temperature, salinity and density equations with multiple models for turbulence
241 (DHI, 2017a). Mike 21 SW is capable of simulating wave growth due to wind action,
242 propagation in deep and nearshore waters, breaking, dissipation, refraction, diffraction and
243 shoaling, non-linear wave-wave interactions, wave-current interactions (refraction,
244 whitecapping), dissipation due to whitecapping, bottom friction and depth-induced wave
245 breaking (DHI, 2017b). The full spectral formulation is based on the wave action conservation
246 equation as described by Komen et al. (1996), and a instationary time formulation has been
247 employed. In case of breaking waves, energy is extracted from the organized wave motion and is
248 converted into turbulence, where the total production of turbulent energy equals the dissipation
249 energy. The eddy viscosity due to wave breaking is calculated from the transport equation for
250 turbulent kinetic energy (e.g. Deigaard et al., 1986; DHI 2017c). Mike 21/3 Coupled Model FM

enables simulation of the mutual interaction between waves and currents using dynamic coupling between the hydrodynamic module and the spectral wave module by including the radiation stress field yieled by the spectral waves simulation that is driving currents in the hydrodynamic module. Also, water levels and current field variations from the hydrodinamic module are included in the wave simulation. Current velocity has to be taken into consideration in calculating wave propagation speed of the wave action (DHI 2017a) as it geneates current-induced refraction. When waves get too steep, the whitecapping dissipation process is accounted for by employing the whitecapping expression of Komen et al. (1994).

Bed shear stress (τ_b) is obtained in the Mike MT module using the Soulsby et al. (1993) maximum current τ_b for flood simulations and maximum combined current and wave τ_b for storm simulations. We use *maximum bed shear stress* because the threshold of motion and entrainment of the sediment are determined by it (Soulsby et al., 1993). Maximum τ_b is usually 2-3 times larger than average τ_b (Soulsby et al., 1993). Numerical aspects and a complete description of the model, with scientific documentation for each module, are available at the Mike website: http://manuals.mikepoweredbydhi.help/2017/MIKE_21.htm#MIKE_21/3_Documentation.

The model simulations and sensitivity tests were calibrated based on field hydrodynamic conditions measured with a Teledyne Workhorse Sentinel Acoustic Doppler Current Profiler (ADCP) in July 2017 and with offshore wave heights from the Gloria Oil Platform. The model was run with calibrated parameters and then with the final flood and storm simulations.

3.3.1 Model calibration and setup

Two simulations were carried out for calibrating the model: (1) hydrodynamic modelling with Mike 3 FM and, (2) wave modelling with Mike 21 SW. A 3D model was chosen due to the importance of stratification in driving hydrodynamics at the river mouth. The first simulation was calibrated for conditions recorded in 28 July 2017 over the Sf. Gheorghe river mouth: Q = 1100 m^3/s; wind speed (*ws*) = 8 m/s, wind direction (*wdir*) = 270°; and the conditions recorded a few hours before the measurements showed a *ws* of 6-10 m/s with *wdir* ~ 0°. The model domain used for calibration covers the NW Black Sea region influenced by the Danube delta with 150 km W-E and 175 km N-S dimensions (Fig. 4A). The model employs an unstructured triangular mesh comprising five levels of grid refinement, with ~ 400,000 elements distributed over 15 vertical uniform sigma layers. The distance between grid nodes at the lowest level is about 45 m. The source of the bathymetry is the GEBCO 2014 30 arc-second grid https://www.gebco.net (Weatherall et al., 2015) for offshore areas with depths > 20 m, and bathymetry measured by the SCMF for shallower waters (2017 for calibration, 2011 for simulations).

To reduce spin-up time for the hydrodynamic simulation, initial conditions of salinity (PSU), temperature (°C) and velocity (m/s) 3D fields were imported from Copernicus Marine, a high-resolution model for the Black Sea http://marine.copernicus.eu/services-portfolio/access-to-products/ (1/27° to 1/36° resolution), 15 days before the ADCP measurements. Daily salinity, temperature, current velocity and sea surface height were added as vertical fields on the E and S boundaries (Flather condition) of the model from the same Copernicus Marine source. Evaporation rates and temperatures were downloaded from Era Interim (https://apps.ecmwf.int/datasets/), and precipitation rates, short wave radiation, long wave radiation, and relative humidity from NCEP/NCAR reanalysis (https://rda.ucar.edu/) were

295 prescribed as 2D fields in the model domain as changes in temperature and salinity can have a
296 small influence.

297 A relatively complex hydrodynamic situation was highlighted during the course of the
298 ADCP survey: a saline intrusion was observed in the river-mouth area. Offshore of the *RMB*
299 crest, a N to S directed buoyant coastal current, the Danubian Current (DC) (Fig. 1B; Fig 5 A,B
300 from 750 to 1500 m offshore) was also detected and was reproduced by the model only when we
301 introduced the influence of the northern Danube river mouths and their buoyant plumes. Buoyant
302 freshwater amplifies the efficiency of wind forcing near the surface (Lentz, 2001) by decoupling
303 the upper buoyant layer from the bottom and thus generating lower shear.

304 The saline intrusion was calibrated by running sensitivity tests and tuning the Vertical
305 Dispersion parameter, which controlled most of the current velocities and structures, and which
306 is based on a scaled eddy viscosity formulation (DHI, 2017a). The default value of 1 was set to
307 0.1 close to the river mouth. To avoid stronger stratification than observed for the offshore zone,
308 we used a value of 0.6 offshore of the *RMB* crest. This agrees best with the measurements which
309 show a strong R (Pearson Correlation Coefficient) of 0.82, a low RMSE of 0.09 m/s, and a slight
310 negative bias of -0.03 cm/s, but led to slight underestimation of the depth of the offshore buoyant
311 coastal current (Fig. 5). Also, a lower bed roughness of 0.02 slightly improved correlation with
312 the ADCP profile. Although we do not dispose of salinity measurements, we observed a good
313 agreement between the observed and modelled velocity fields, which implied that the salinity
314 fields were also correctly modelled (Fig. 5 A, B).

315 The calibration mesh for waves is of lower resolution (excludes first 3 levels near the
316 river mouth), due to the long simulation time (6 months), and because it was not necessary to
317 include detailed nearshore cells. Mike 21 SW was calibrated for waves measured at the Gloria

318 Oil Platform for a total of 6 months. The Gloria record contained two of the most severe storms
319 in the NW Black Sea (January 1998 and January 2004) over the period of measurement, with
320 local wind data from the Gloria wind station (adjusted at an elevation of 10 m after Rusu et al.,
321 2014). ERA Interim data (*Hs*, wave period, *wdir*, directional standard deviation) were prescribed
322 at the E and S boundaries. The model included quadruplet interactions, due to the importance of
323 this process for deep water waves. Default conditions resulted in slightly lower extreme wave
324 heights, and as such, we lowered the Coefficient of Dissipation (Cdis) for whitecapping from a
325 default of 4.5 to 4. For the nearshore, we used the Nikuradse roughness value of 0.02
326 recommended by the Halcrow report for the Romanian coast (Halcrow, 2011). The final run
327 resulted in very good agreement of modelled and measured wave heights R=0.93, correctly
328 estimating slope of the relationship and the extreme wave heights (Fig. 5C): the RMSE is 0.33 m
329 (0.29 for the mean normalized RMSE) and the bias is low (0.06), similar to what other studies
330 obtained for the NW Black Sea (e.g. Rusu, 2015).

331

332 *3.3.1 Flood and storm simulations and setup*

333

334 Different thresholds of low, medium and high discharge (*Q*: 1000, 2200, 3200, 4000
335 m^3/s) and wave height (H_s: 1.5, 2.5, 4, 6 m) corresponding to different percentiles were modelled
336 with the Mike model in order to investigate the hydrodynamics during floods and storms. We
337 used for the flood and storm simulations a high-resolution, 3-level mesh with ~680,000 elements
338 distributed in 20 uniform vertical sigma layers, and a distance of about 30 m between the
339 triangulated grid nodes in the most detailed level and an element surface of ~650 m^2 (Fig. 4B).
340 The river channel was prescribed with a quadrangular grid to improve flow at boundary

conditions due to errors appearing from the use of sigma layers. Higher order solutions for time and spatial integration, a horizontal eddy viscosity Smagorinsky formulation (0.28), and a vertical - k-epsilon model for turbulence were employed, the effect of Coriolis included and Flather conditions prescribed at open boundaries.

We ran simplified flood simulations in Mike 3 FM, neglecting the influence of wind, waves and of the northern Danube river mouths, with increasing Q which reached a maximum of 4000 m^3/s. Flood simulations were initialized with averaged salinity fields for the month of April 2005 from Copernicus Marine; temperature influence was excluded, and the model ran for one week for each condition. Hydrodynamic conditions seem to have reached a stable point of diminishing change at the end of the week in the absence of mixing due to winds and waves.

The storm simulations were run in coupled Mike 3 FM and Mike 21 SW modules with typical conditions of Q (1250 m^3/s) that appear to be most common during storms in December - February. In the final storm simulation, baroclinic effects were excluded because of the low impact on circulation during storm conditions (Fig. 3). The storm was modelled as a whole event with 12 hour per wave threshold and fixed 45° direction specified at the open boundaries, thus mimicking realistic increase in the peak of the storm which occurs in one or a few days. The currents generated were combined wind and wave currents, and the wind was prescribed with 8, 12, 17, 25 m/s following a relationship between *Hs* and *ws* at the Sulina weather station (Fig. 1). The storm simulation included diffraction, triad and quadruplet wave interactions, a wave breaking approach based on the functional form of Ruessink et al. (2003), bottom friction Nikuradse roughness of 0.02, and a whitecapping Cdis coefficient of 0.4 obtained from calibration. It should also be noted that the model is not calibrated for depth-limited breaking. The SW simulation employed a logarithmic discretization of 25 frequencies whereas the wave

action spectrum was discretized in 12 directions on a 0 to 180 degrees directional sector, which resulted in a 15° resolution, sufficient for wind waves. We also reduced the maximum number of levels in transport calculation to 4, necessary in conditions with strong wave breaking.

4 RESULTS

In the following sections, each analyzed time period between successive measurements is named based on the last year of measurements, such that 2004-2005 becomes T_{05}…. and 2017-2018 becomes T_{18}. We first describe the relationship between bathymetric change and flood and storm forcing.

4.1 Bathymetric change and hydrodynamic forcing

A whole range of bathymetric changes was recorded over the 2004-2018 period (Fig. 6; Suppl. 2). The net difference in volume of the river mouth area between two successive measurements (ΔV) ranged from equilibrium (ΔV ~ 0), to moderate (ΔV: ± 0.5 to 2 × 10^6 m^3) and extreme ΔV: +5.2 × 10^6 m^3 (T_{06}) to -6.8 × 10^6 m^3 (T_{12}). Considered extreme periods T_{06} (positive) and T_{12} (negative) are around a distance of 2 standard deviations from the mean. Accumulative and erosive periods show opposite morphodynamic patterns. Both are characterized by a zone of high ΔV in the immediate vicinity of the river mouth at 4 to 8 m depth and decreasing ΔV further offshore, alongshore and inside the Danube channel, but with opposite signs (Fig. 6).

The T_{05} (ΔV = 3 × 10^6 m^3) and T06 (ΔV = 5.2 × 10^6 m^3) periods are dominated by the occurrence of exceptional floods that peaked at 3500 and 4000 m^3/s respectively, during

moderate storminess (Fig. 7A, B, C). Under these conditions, the *RMB* crest migrated offshore by ca. 300 m, as a cumulative effect of the succession of two extraordinary hydrological years, and the depositional layer varied from a maximum of 1 – 3 m on the seaward side of the *RMB* crest to about 0.5 – 1 m offshore to the prodelta. Slight erosion (≤ -0.5 m) occurred in the river-mouth channel. Moderate flood years showed similar patterns (offshore mouth-bar migration, offshore deposition), but of lower magnitude. Nevertheless, during the low flood and low storm periods (T_{07}, T_{08}), 65% of the new deposed sediment (ΔV: T_{05}+T_{06}) was removed.

A large sediment volume ($\Delta V = -6.8 \times 10^6$ m^3), comparable to that recorded post-major floods, was swept away during T_{12}, a year characterized by multiple episodes of high waves (H_s > 4 m) and an extreme storm (H_s > 6 m) that lasted from 5 to 10 Feb 2012. The largest erosion in T_{12} occurred up to -8 m depth on the seaward side of the protruding *RMB* crest, with extreme erosion values reaching the -2 to -4 m depth interval. Offshore, the bed-level changes varied from -1 m at the base of the crest to -0.5 m. Accumulation occurred only in the Danube channel. During low to moderate storm years the maximum erosion zone affected constantly the mouth bar crest, linked to low-to-moderate waves breaking on the protruding crest. The *offshore* zone experienced a low but still noteworthy morphological change (-0.1 to -0.5 m). As total erosion increased, the maximum erosion depth moved offshore.

It is also obvious that total ΔV was highly influenced by the strength of the hydrodynamic forcing: the highest positive ΔV occurred during the exceptional flood years, and the highest negative ΔV during the extreme storm year. These results throw light on the high morphological variability that can occur at wave-influenced river mouths, driven by the variability and timing of forcing events.

410 4.2 Flood/Storm index

411

412 To relate morphological changes to the forcing, we propose a Flood/Storm index (FL/ST_i)
413 that can be computed using proxy data: FL/ST_{dur} is the ratio of the duration of floods (Q) and
414 storms (H_s) above a certain threshold (see Table 1 for threshold definition; and the discussion
415 chapter 5.2 for the rationale for using this index):

416 $$FL/ST_{dur} = \frac{Q_{75}}{H_{s98}} \quad (3)$$

417 where Q_{75} = duration of discharge above the 75th quantile, H_{s98} = duration of significant wave
418 height above the 98th quantile, and FL/ST_{sed} the ratio of sediment discharge above 125 kg/s and
419 cumulative storm wave power above $H_{s2.5}$ (significant wave height of 2.5 m).

420 $$FL/ST_{sed} = \frac{Q_s}{Wp} \quad (4)$$

421 where, Q_s = total sediment discharge > 125 kg/s (50th quantile), and Wp = cumulative storm
422 wave power above the 98th quantile.

423

424 Wave power calculations were based on Moritz and Moritz (2006). *FL/STi* is calculated
425 for quasi-yearly periods representing intervals between the analyzed bathymetric measurements.
426 Thresholds were chosen by finding the quantiles that yielded the highest correlation with
427 measured ΔV. Thus, the Q_{75} (the duration of discharge above the 75th quantile or 2200 m^3/s for
428 the Sfântu Gheorghe branch) and the H_{s98} (the duration of significant wave height above the 98th
429 quantile or 2.5 m) were found to be most representative. Q_{75} is the highest flood quantile with
430 durations >0 for every measurement interval. It was also necessary to use a threshold for

sediment discharge to obtain the best correlation; this was Q_s = 125 kg/s, the Q_s average for the Sf. Gheorghe being ~ 160 kg/s. This requirement can be explained by bedload transport which results in the mobilization of sediment from the river channel into the mouth area and which is insignificant outside medium and high discharge conditions, and by a possible increased flocculation rate during floods, a process hinged on particle collision rate (Winterwerp and van Kesteren, 2004). It is expected that the FL/ST_{dur}, which uses only liquid discharge (Q), is only valid when the Q and Q_s relationship remains unchanged. FL/ST_{dur} and FL/ST_{sed} show good correlation with the measured budget changes, with R^2 of 0.8 and 0.84, respectively, for the whole river-mouth area and R^2 of 0.79 and 0.75 for the RMB_{crest} (Fig. 8).

Even though the overall correlation is good, there may be some significant differences between measured and predicted ΔV which can amount to more than 1×10^6 m^3/yr during certain years. In 5.1.1 and 5.1.2, thresholds are discussed in relation with the corresponding hydrodynamics, and may shed some light on the ΔV complexity which is not taken into account by this approach.

4.*3 Extreme events*

4.3.1 Floods

Simulations with different discharge levels (Q_{15} to $Q_{99.7}$, see table 1 for Q thresholds), and no wind or wave influence, reveal that the circulation in these conditions is dominated by changes in Q, the interaction of flow with bathymetry, and buoyant effects due to the differences in salinity (Fig. 9A, B). The circulation is highly stratified, exhibiting a clear hypopycnal regime. In the

454 absence of enhanced mixing by winds and waves, there is a sharp horizontal salinity gradient
455 delimiting the buoyant river jet and plume from the Black Sea waters.

456 The plume liftoff, i.e. the hydraulically forced detachment of buoyant freshwater from the
457 channel bottom or seabed (Poggioli and Horner Devine, 2018) occurs close to the river mouth,
458 and marks the start of the rapidly expanding buoyant plume (Fig. 9). The liftoff point is inside
459 the river channel for low discharges, i.e. Q_{15} (1000 m^3/s), which allows for the upriver saline
460 intrusion, and jumps over the *RMB* crest with increasing Q. Diminishing offshore displacement
461 is observed with increasing Q: the liftoff point location at Q_{95} is not much different from $Q_{99.7}$.
462 Plume liftoff location is important in generating an area of lower flow close to the bed and as
463 such, a sharp decrease in τ_b. Further implications of the plume liftoff point, and the secondary
464 circulation on sedimentation will be treated in the discussion.

465 The large discharge during floods, flowing through a relatively narrow channel outlet
466 (500 m width, 5 m depth), creates strong frictional effects on the *RMB* when depth decreases to
467 1.5-2.5 m. Frictional effects with the *RMB* bed and especially with its crest cause jet spreading
468 and current deceleration. The main morphological features (bathymetry and river channel
469 orientation) generate preferential steering to the right of the current, complemented further
470 downdrift by Coriolis and Coandă effects.

471 Simulations for Q_{75} (2200 m^3/s), Q_{95} (3200 m^3/s) and $Q_{99.7}$ (4000 m^3/s) discharges show
472 the Sf. Gheorghe turbulent river jet and plume dynamics during typical and extreme flood
473 conditions. Velocities for Q_{75} rapidly decrease from 1 m/s to 0.5 m/s immediately after the *RMB*
474 crest and to 0.2 m/s offshore, and increase for $Q_{99.7}$ at 1.8 m/s in the river channel, 0.6 m/s after
475 the *RMB* crest and 0.4 m/s offshore. There is a marked decrease in the surficial current velocities

476 (of 20-30%) at the plume liftoff point, and then a similar increase in velocities after the *RMB*
477 crest due to the convergence with the secondary bottom current directed onshore (Fig. 9A, B).
478
479 *4.3.2 Storms*
480
481 The combined fluvial jet current and longshore current (*LSC*) was simulated for different
482 H_s thresholds ($H_{s1.5}$ to H_{s6}), at fixed 45° direction and Q discharge of 1250 m^3/s (Fig. 9). Waves
483 start breaking on nearshore bars and on the *RMB* crest to generate the longshore current (*LSC*),
484 which is responsible for longshore sediment transport (*LST*). The *LSC* at $H_{s1.5}$ appears as a weak
485 current, mostly present on the first (proximal) and second bars at the updrift and downdrift coasts
486 with velocities of ~ 0.5 m/s (Fig. 10). The northern *LSC* discharges into the river outlet, whereas
487 the *LSC* generated over the *RMB* crest passes over it due to the lower depths < 2 m and to the
488 protruding, curved isobaths at the northern part of the *RMB*. Further south (Fig. 10, 4971500) the
489 border between the *LSC* and river jet is not clear, although there is an enhancement in flow at the
490 outer edge of the river jet at the *RMB* crest (Fig. 10A, B). As wave heights increase, wave
491 breaking occurs at progressively greater depths, the dissipation zone widens, and the *LSC* mostly
492 grows by extending its influence offshore. The *LSC* appears to be on the *RMB* crest at $H_{s1.5}$ (Fig.
493 10B). Waves start breaking at $H_{s2.5}$ on the distal bar on the northern shoreface, and with
494 increasing depths (H_{s4}, H_{s6}) on the upper shoreface slope outside the nearshore bars. As such,
495 maximum velocities are attained at depths of ca. 2 m ($H_{s1.5}$), 4 m ($H_{s2.5}$), 6 m (H_{s4}) and 8 m (H_{s6})
496 and range from 0.5 m/s ($H_{s1.5}$) to 2 m/s (H_{s6}) (Fig. 10). *LSC* in $H_{s2.5}$ appears discharging partly
497 into the river mouth area, but mostly passing over the *RMB* crest, whereas complete bypassing of

498 the *RMB* is noticed only with higher H_s. Most of the high waves are dissipated before arriving at
499 the lower depths (Fig 10C) and this explains the offshore increase in current velocities.
500 The circulation is alongshore-dominated, with a highly downdrift-deflected river jet even
501 at $H_{s1.5}$. The *LSC* interacts with the river jet, although much of the *LSC* over the *RMB* is
502 explained by the morphology of the latter. Nevertheless, the jet appears to have some effect on
503 the river-mouth hydrodynamics, tempering current velocities in the northern part of the river
504 outlet (Fig. 10A). Although not investigated here, higher Q is expected to enhance this effect.
505 Downdrift of the river outlet, the combined jet - *LSC* velocities increase with higher H_s.
506

507 ## 5. DISCUSSION

508

509 The fate of sediment dispersed from the river into the coastal ocean involves at least four
510 processes: supply via plumes, initial deposition, re-suspension and transport by marine processes,
511 and long-term net accumulation (Wright and Nittrouer, 1995). At present, most of the deposited
512 sediment in the Sf. Gheorghe river-mouth area can be quickly remobilized in the following
513 months and years, regardless of the occurrence or not of high storm waves ($H_s \geq 4$m). As such,
514 this river-mouth area functions as a temporary depocentre, with most of the captured sediment
515 being then remobilized and transported to the south. The following discussion aims at clarifying
516 the deposition and resuspension processes and at linking measured morphological change with
517 the hydrodynamic data, obtained with the aid of numerical modelling with the Mike 21/3, in
518 order to derive a conceptual hydro-morphodynamic model of an asymmetric wave-influenced
519 river-mouth bar during the two antagonistic phases: (1) flood-dominated; (2) storm-dominated
520 (Fig. 11).

521

522 *5.1 Processes explaining sediment deposition and erosion patterns*

523

524 *5.1.1 Floods*

525

526 Floods are characterized by large increases in Q and Q_s at the river mouth which generate
527 changes in hydrology and, ultimately, in the topography of the bed. Interactions between the
528 river effluent with bathymetry and buoyancy effects govern the spreading rate of the river jet, the
529 plume liftoff point, and the bottom plume return current, and ultimately, sedimentation patterns.
530 Sediment settling from the plume produces a seaward-thinning and seaward-fining depositional
531 wedge, which reflects the processes involved in sediment transport and deposition (Fig. 6: T_{05},
532 T_{06}; Fig. 11). The recorded volumes and bed change in the course of T_{05} and T_{06} are remarkably
533 similar to the volumes and bed changes during the exceptional 2004 Rhône flood (Maillet et al.,
534 2006) which peaked at 12,000 m^3/s but lasted only a few days.

535 Stratification is responsible for a reduction in turbulence which can increase the trapping
536 rate by an order of magnitude for silt-size sediment particles (Geyer, 1993). The plume return
537 flow present even during high river discharge contributes in retaining sediment near the shore, as
538 in the case of the Mekong (Eidam et al., 2017). The bottom convergence of flow at the plume
539 liftoff zone is a pervasive and important mechanism for trapping sediments and maintaining the
540 turbidity maximum in estuaries (Schubel and Carter 1984; Dyer 1995; Burchard and Baumet
541 1998; Geyer et al., 2004). In a modelling study, Thanh et al. (2017) explored suspended sediment
542 dynamics with or without salinity gradients and found that suspended sediments are deposited
543 significantly more rapidly nearshore when salinity gradients are present. This is attributed to two

544 mechanisms: the onshore bottom circulation (the plume return flow), and the inhibition of
545 sediment spread throughout the vertical water column caused by a reduction in the vertical
546 diffusivity. Even though the plume return flow has low velocities (0.1 - 0.2 m/s) its depth is a
547 few times larger than the buoyant plume above, and this suggests that the former, when present,
548 may greatly favour sequestration. Modelling on the Danube delta coast in realistic conditions
549 showed that increased discharge and increased mixing due to wind push seaward the plume
550 liftoff point to larger depths, thus, reshaping the interaction of the surface plume current and the
551 plume return flow (Bajo et al., 2014), although high stratification may still take place even
552 during extreme flood discharges, as in the case of the Po (Tesi et al., 2011). Notably, the
553 modelled plume liftoff zone is in agreement with the maximum sediment deposition recorded at
554 the Sf. Gheorghe mouth (Fig. 6, T_{05}, T_{06}; Fig. 9A). The bedload and resuspended sands from
555 inside the *RMB* channel due to high τ_b (Fig. 9D) may have contributed significantly to the
556 deposition just outside the *RMB* crest when τ_b decreases abruptly (Anthony 2015a), and fostered
557 the large migration of the *RMB* crest during T_{05} and T_{06} (Fig. 6). Additionally, the lower τ_b after
558 the mouth bar crest ensures the preservation of both sands and silts settling over the bed,
559 generating and preserving the *RMB* sand-silt lamination signature. Mapping of grain-size
560 parameters (Fig. 2B) following flood conditions (summer of 2005 and 2006) shows persistent
561 patterns of sand-mud transition in which the contact between the two fractions occurs at -6 m to -
562 8 m in the central sector, and rises to -3 m to -4 m on the lateral northern and southern flanks, in
563 accordance with the position of the liftoff point and the vertical distribution of the current speeds
564 (Fig. 9B, C). It is noteworthy to question the southern limit of the sandy surficial cover which
565 marks the shortest transition from sands to fine silts and clays (100-150 m), and which occurred
566 on relative flat or gently sloping surfaces in the absence of any prominent features (crests,

slopes). Moreover, a 300-400 m wide band of fines occur immediately seaward of the bar zone on the southern (downdrift) coast. This grain-size pattern matches well with the current speed simulations during floods (Fig. 9B) and with the measured deposition (Fig. 6), and seem to be the combined effect of current deceleration and convergence with the plume return flow and of flocculation.

Flocculation processes can significantly restrict transport distances and enhance deposition of silts and clays near river mouths (Dalrymple and Choi, 2007; Hill et al., 2000; Fox et al., 2004a; Milligan et al., 2007, Geyer et al., 2004; Nowacki et al., 2012). The net result is an overall increase in the size and settling velocity of the fine-grained material. Flocculation can increase the falling velocity of particles by several orders of magnitude (Kranck, 1980), and can induce settling velocities in excess of 1 mm/s (Fox et al., 2004a; Milligan et al., 2007). The Po river plume loses most of the suspended load within 1–2 km of the mouth (Fox et al., 2004b). Constantin et al. (2017) found that the spatial extension of the Danube sediment plume is limited to high turbidity close to the river mouths. The interbedded sand-mud deposits that form the river-mouth bar suggest intense flocculation processes even close to the river mouth (Fig. 2B), akin to those of the low-energy shelf setting of the Po (e.g., Fox et al., 2004a; Tesi et al., 2011). Nevertheless, deposition of a few cm can be recorded after floods even at >30 m depth (Frascari et al., 2006) or 10 km offshore of the river mouth (van Maren and Hoekstra, 2005). The offshore edge of our study area (-16 to -20 m), recorded a maximum of 20 to 50 cm bed change, suggesting significant deposition on the prodelta as well.

Sediments from floods are expected to reach greater deposition depths due to increase in sediment residence time caused by increased plume thickness and plume velocity (Milligan et al., 2007; Geyer et al., 2000). Additionally, strong wind-generated currents and wave-induced

590 turbulence during summer may act to hinder sedimentation and break flocks (Dalrymple and
591 Choi, 2007), and to provide momentum in generating buoyant coastal currents that favour
592 sediment transport. During windy conditions, an episodic buoyant coastal current, connected to
593 the Danube mouths, enhances mixing and circulation alongshore (Fig. 5 A, B; Dinu et al., 2013).
594 Additional complexity in sediment retention during floods is expected from interaction with
595 buoyant coastal currents formed at adjacent river mouths and with episodic wind and wave
596 events.
597
598 *5.1.2 Storms*
599
600 During storm conditions, waves control resuspension and sediment transport (Dufois et
601 al., 2014), and usually create shear stresses of an order of magnitude higher than currents (Harris
602 et al., 2008). With decreasing depths, the bed is exposed to increasing circular orbital motion
603 which also becomes more elliptical close to the bed (Knauss, 1997), leading to greater near-bed
604 wave orbital velocities up to the breaking point (Pratson et al., 2007). Wave resuspension and
605 current transport act in concordance, and most of the resuspended sediment travels in dilute
606 suspension downdrift. The different effects of waves, currents, and different sediment grain sizes
607 at the Sf. Gheorghe river mouth can be roughly approximated to occur in two scenarios: (i)
608 combined *LSC*, wave shear stresses and wave breaking acting on a predominantly sandy bed
609 (surf zone); ii) combined *LSC* and wave stresses acting on a predominantly fine sediment bed
610 (lower shoreface, prodelta) (Fig. 10).
611 Although defining critical shear stresses (τ_{b_crit}) requires caution (Vanoni et al., 1964), a
612 value of 0.9–1.6 τ_{b_crit} seems to be sufficient to explain the resuspension and transport of very

fine sand as suspended load (van Rijn, 1984; Nowacki et al., 2012). Furthermore, studies in natural settings appear to be in relative agreement that a threshold τ_{b_crit} of silt is around 0.2 to 0.4 N/m^2 (Xu et al., 2014; Sha et al., 2018). When sediment is suspended at τ_b of 0.2 N/m^2, the quantities involved are limited (Xu et al., 2014), whereas fine sediments exposed to high shear stresses (τ_b > 2 N/m^2), may shift the bed into a more erosive state (Amos et al., 1992), indicating that increase in τ_b strongly correlates with increasing sediment remobilization rates. It seems that $H_{s1.5}$ conditions permit fine sand resuspension on the shoreface, and limited fine resuspension from the lower shoreface (Fig. 10D), whereas τ_b for > $H_{s2.5}$ can significantly remobilize fines from deeper waters. Stronger *LSC* velocities and τ_b increase and extension are in agreement with the increased erosion occurring at the *RMB* during storm-dominated periods (Fig. 11; Fig. 7, T_{12}, T_{17}), and explain the changes in the recorded morphology. Preliminary morphological simulations with Mike MT (Mud transport Module) for the Sf. Gheorghe river mouth show that the bed erosion that occurred in 2011-2012 can be explained only by including in the model fine sediments which are dominantly eroded in deeper areas (Zăinescu et al., 2018). Comparatively, "only sand" simulations differed in both patterns and magnitude with the measured data. This is not surprising, as sedimentological data based on shallow cores and surface samples show that cohesive sediments are dominant below -4 m to -8 m depths in front of the river mouth (Fig. 2B), with some seasonal variations. Most of the world's large deltas are dominated by fine-grained sediment debouching at their mouths, and there is a need to pay greater attention to the morphodynamic significance of these fine sediments at wave-influenced delta fronts.

Cross-shelf transport to greater depths has been found to occur due to gravity-driven flows (wave-assisted) resulting from wave-induced suspension that maintains thin near-bed turbid layers during storms (Cacchione et al., 1999; Ogston and Sternberg, 1999; Wright et al.,

1999; Nittrouer, 1999; Harris et al., 2005; Falcini et al., 2012). This is observed mostly for dispersal-dominated systems (cf. Walsh and Nittrouer, 2009) but has also been recognized for the Po delta, a proximal-accumulated-deposition (PAD) system (Traykovski et al., 2007), similar to the Danube dispersal system. Nevertheless, alongshore sediment transport due to wave resuspension and wind-forced mean currents was an order of magnitude larger than cross-shore flux associated wave-supported gravity flows (Traykovski et al., 2007), which may indicate that most sediment near the Sf. Gheorghe river mouth is transported alongshore by currents in the form of dilute suspension, similar to the Po (Nittrouer et al., 2004; Traykovski et al., 2007), although the model in the present paper still needs more calibration with in-situ measurements. However, downslope transport is not excluded by strong isobath-parallel currents (Ma et al., 2008). Some dispersal systems may thus be more alongshore-dominated (e.g. PAD systems) whereas on other systems, which are more wave-dominated, down-slope wave-supported gravity flows may have a larger contribution. Submarine slides and slumps have been identified in front of the Sf. Gheorghe river mouth using a sidescan sonar (Alexandru Ionescu, Marine Research – pers. comm.). Similar mass failures are present on the Rhône (Maillet et al., 2006) and Po (Bosman et al., 2014) river mouths, albeit with apparently secondary influence on cross-shore transport. Compaction and the action of waves on sediments of different consolidation (Guillén et al., 2006), and biological processes enhancing or limiting erodibility (Xu et al., 2014), should add a further degree of complexity to bed response during storms.

5.2 The importance of extreme events and insight from the Flood/Storm index:

658 The cycling processes of flood deposition and storm resuspension of sediments are
659 embedded in the very nature of deltas. At the Yangtze river mouth, monthly deposition rates
660 during flood periods are an order of magnitude higher than long-term accumulation rates, which
661 suggests that a major portion of the river-derived sediment is eroded periodically (Liu et al.,
662 2007). The net 2018-2004 bed change at the Sf. Gheorghe river mouth is much lower than would
663 be the combined yearly changes measured at this river mouth (Suppl. 2). A stratigraphic analysis
664 of the asymmetric wave-influenced lobe of the Brazos delta (Gulf of Mexico coast) has shown
665 that flood deposition and storm resuspension are an integral part of the resultant stratigraphy,
666 (Rodriguez et al., 2000), leading these authors to propose that the Brazos delta is a "flood-and-
667 wave" feature, with some degree of control from large-scale climatic teleconnection cycles
668 (Fraticelli 2006). Reductions in flood frequency caused significantly less deposition at the Rhône
669 river mouths (Provansal et al., 2015). It seems thus that the interplay between floods and storms,
670 as suppliers and removers of sediment at river mouths, drives most of the morphological changes
671 in many delta river-mouth systems. In turn, changes in flood and storm frequency and magnitude
672 are driven by either natural variability or anthropogenic causes, the effects of which can greatly
673 influence deltaic morphodynamics on many timescales.

674 Predicting deltaic morphology with simple indexes based on relative ratios of
675 oceanographic vs riverine forcing has always been tempting for coastal researchers, as shown by
676 the diversity of deltaic indexes. First attempts by Wright and Coleman (1973) linked river- and
677 wave-dominated delta morphology to water discharge and wave power, and were followed by
678 Galloway (1975) who proposed the famous tripartite scheme with the inclusion of tidal effects.
679 The Asymmetry Index (A), proposed by Bhattacharya and Giosan (2003), explores the
680 asymmetry controlled by the *LST* and *Q*. Further studies established simple conceptual

representations of the sediment balance at river mouths, which is envisaged in terms of the sediment arriving at the mouth (Q_s) versus the magnitude of the *LST*. These are the fluvial dominance ratio (R) (Nienhuis et al., 2015), which predicts deltaic plan shape morphology, and the sedimentary index (Si) (Preoteasa et al., 2016), which can capture the increase in the influence of wave-driven sediment circulation on river mouth morphology occurring in the past centuries at the Sf. Gheorghe river mouth.

The FL/ST index applied in this study reveals that river mouth ΔV responds according to flood and storm variability. Most importantly, the index shows that for the investigated time period there is a linear response of bathymetric changes in relation to the relative influence of flood and storm events in spite of the bewildering complexity of the river-mouth environment (Anthony, 2015a). This index has the advantage of using simple data of offshore H_s, as opposed to *LST*, which may be difficult to compute and which ignores fine sediment resuspension. As a rule of thumb, the index suggests that for every 1 hour of $H_s > 2.5$ m, 15 hours of $Q > 2200$ m^3/s at the Sf. Gheorghe river mouth are needed to counterbalance the sediment removal by storms. This suggests that the observed bathymetric yearly changes are largely the result of the cumulative effects of storm and flood events. These variations are further accentuated where flood years and high storminess years are negatively correlated, such as in the sf. Gheorghe case. At least for this river mouth where floods and storms occur asynchronously, hydrodynamic interactions at the river mouth are not of first order significance (Fig. 2C; Fig. 3). The timing of these events is largely governed by continental-scale constraints, whereas smaller river basins are more likely to experience both floods and storms at the river mouth from the same atmospheric disturbance. Currently, the effects of storm and flood timing, either synchronous (e.g. Rhône:

703 Boudet et al., 2017), asynchronous (e.g. Danube, Mekong: Thanh et al., 2017) or mixed (e.g. Red
704 River: van Maren and Hoekstra, 2005) are not clear.
705
706 Q_{75} and H_{s98} events can account for most of the variability produced in the river-mouth
707 area ($R^2 = 0.84$). This is unsurprising as floods are responsible for most of the sediment transport
708 in rivers (Marion et al., 2010), and higher waves ($\geq H_{s2.5}$) are necessary to explain the higher
709 erosion of the bed at the lower shoreface, whereas waves as low as < Hs 1.5 m may not be able
710 to apply sufficient τ_b. In addition, since longshore transport formulas describe a power-law
711 relationship between wave heights and *LST* magnitude, a doubling in Hs causes an order of
712 magnitude increase in longshore sediment transport in most formulas (Mil-Homens et al., 2013;
713 van Rijn 2014; Shore Protection Manual, 1984), without losing view of the fact that further large
714 variability in LST magnitude can be caused by slight variations in other input parameters (Pinto
715 et al., 2006).
716 *RMB* variability response to a $H_{s2.5}$ threshold, in comparison with including the *Wp* for a
717 whole year, may be explained by a balance between frequency and impact of these events.
718 Validity of a similar threshold for other study sites may be possible, especially for wave-
719 influenced river mouths in similar conditions, which are abundant in the Mediterranean basin
720 (Besset et al., 2017). Nevertheless, the relationship embodied in FL/ST_i may be susceptible to
721 change at longer timescales due to morphologic adjustments of the river-mouth area.
722

723 ## 6. CONCLUSIONS

724

725 The morphological evolution of a wave-influenced river mouth was monitored over the
726 last 15 years, and the observed changes related to external forcing. Simplified conditions for
727 hydrodynamic modelling during relevant flood and storm thresholds revealed the main processes
728 responsible for morphological change. Nevertheless, the complexities and exact contribution of
729 the resulting circulation that can be attributed to each process in sediment transport still remains
730 open for future studies. There is a need to know where the totality of the sediment during floods
731 gets deposited, how this deposition is affected by wind-influenced processes during the flood
732 season, and what the role of stratification is in sediment deposition close to the mouth. For
733 storms, there is still a knowledge-gap on the contribution of fine sediments to delta-front
734 morphodynamics. Moreover, the question of where the sediment gets redistributed after removal
735 from the river mouth area is still a question open to debate, with some studies indicating sand
736 trapping in spits as possible effective mechanisms of deltaic reorganization (Nienhuis et al.,
737 2013; Anthony 2015b; Besset et al., 2017), although this suggestion is not based on a complete
738 assessment of sediment budgets. Nevertheless, aspects such these govern the response of deltas
739 to changes in Q_s, storminess, and sea-level rise, and should spark further research interest.
740
741 The conclusions from our investigation are summarized as follows:
742
743 (1) A conceptual model was derived that emphasizes the role of floods and storms in
744 driving morphological change at the river mouth.
745 (2) During floods, a seaward-thinning depositional wedge is formed (from a few m to
746 cm-scale) that is related to plume transport and sediment settling.

747 (3) During storms, high bed shear stresses (τ_b) generated by combined currents and waves
748 remove the sediment deposited during floods.
749 (4) A new proposed index (*FL/STi*) based on storm and flood thresholds explains the
750 sediment budget variability at the Sf. Gheorghe river mouth and reveals a linear response in
751 bathymetric change to the relative influence of storms and floods.
752

753 **ACKNOWLEDGEMENTS**

754

755 FZ undertook part of the work at Aix-Marseille University under a "Bourse du gouvernement
756 français" PhD cotutelle thesis awarded by the Institut Français de Roumanie, and benefited from
757 the MIKE Powered by the DHI thesis programme which permitted using all Mike modules free
758 of charge. Daily liquid discharge and monthly sediment discharge were made available by the
759 National Institute of Hydrology and Water Management (INHGA) in Romania. We would also
760 like to acknowledge the work of our colleagues Ștefan Constantinescu, Daniel Ivanov, Nichita
761 Nicolae from the Sfântu Gheorghe Fluvial and Marine Research Station which contributed to the
762 bathymetrical monitoring programme of the river mouth. We thank two anonymous reviewers
763 and Editor-in-Chief Shu Gao for their insightful comments.

764
765
766
767
768
769

REFERENCES

Allison, M. A., Kineke, G. C., Gordon, E. S., Goni, M. A., 2000. Development and reworking of a seasonal flood deposit on the inner continental shelf off the Atchafalaya River. *Continental Shelf Research*, 20, 2267-2294.

Amos, C. L., Daborn, G. R., Christian, H. A., Atkinson, A., Robertson, A. N. D. A., 1992. In situ erosion measurements on fine-grained sediments from the Bay of Fundy. *Marine Geology*, 108, 175-196.

Anthony, E. J., 2015a. Wave influence in the construction, shaping and destruction of river deltas: A review. *Marine Geology*, 361, 53-78.

Anthony, E.J., 2015b. Deltas. In: Masselink, G., Gehrels, R. (eds.), Coastal Environments and Global Change. John Wiley & Sons Ltd., pp. 299–337.

Bajo, M., Ferrarin, C., Dinu, I., Umgiesser, G., Stanica, A., 2014. The water circulation near the Danube Delta and the Romanian coast modelled with finite elements. *Continental Shelf Research*, 78, 62-74.

Besset, M., Anthony, E. J., & Sabatier, F., 2017. River delta shoreline reworking and erosion in the Mediterranean and Black Seas: the potential roles of fluvial sediment starvation and other factors. *Elementa, Science of the Anthropocene*, 5, 54, https://doi.org/10.1525/elementa.139.

Bhattacharya, J. P., Giosan, L., 2003. Wave-influenced deltas: Geomorphological implications for facies reconstruction. *Sedimentology*, 50, 187-210.

Blöschl, G., Nester, T., Komma, J., Parajka, J. and Perdigão, R.A., 2013. The June 2013 flood in the Upper Danube Basin, and comparisons with the 2002, 1954 and 1899 floods. *Hydrology and Earth System Sciences*, *17*(12), pp.5197-5212.

794 Bondar C., State I., Cernea D., Harabagiu E., 1991. Water flow and sediment transport of the
795 Danube at its outlet into the Black Sea. Meteorology and Hydrology, 21.1, p. 21-25, Bucuresti.
796 Bondar C., Borcia, C.,Rădulescu, C., 2011. Aspects on the extreme phenomena in Danube
797 Mouths Area and in the Black Sea Coastal Area. In: Proceedings of the Annual Scientific
798 Conference INHGA, pp.209–228.
799 Bondar, C., Iordache, G., 2016. Sediment transport on the Romanian section of the Danube river.
800 GeoEcoMarina, (22).
801 Bondar, C. and Panin, N., 2001. The Danube Delta hydrologic database and modelling. GeoEco-
802 Marina 5–6, 5–52
803 Bornhold, B.D., Yang, Z.S., Keller, G.H., Prior, D.B., Wiseman, W.J., Wang, *Q*., Wright, L.D.,
804 Xu, W.D., Zhuang, Z.Y., 1986. Sedimentary framework of the modern Huanghe (Yellow-River)
805 Delta. Geo-Mar. Lett. 6 (2), 77–83.
806 Bosman, A., Madricardo, F., Remia, A., Correggiari, A., Romagnoli, C., Kruss, A., A.,
807 Casalbore, D., Morelli, E., Moscon, G., 2014). First morphological mapping of the Po delta
808 (North Adriatic Sea, Italy) from ultra high-resolution multibeam bathymetry and backscatter
809 data. In Conference Paper. Ocean Sciences Meeting Hawaii Convention Center. Honolulu,
810 Hawaii USA.
811 Boudet, L., Sabatier, F., Radakovitch, O., 2017. Modelling of sediment transport pattern in the
812 mouth of the Rhone delta: Role of storm and flood events. *Estuarine, Coastal and Shelf Science*,
813 198, 568-582.
814 Boyd, R., Dalrymple, R.W., Zaitlin, B.A., 1992. Classification of clastic coastal depositional
815 environments. *Sedimentary Geology*, 80, 139-150.

816 Burchard, H., Baumert, H., 1998. The formation of estuarine turbidity maxima due to density
817 effects in the salt wedge. A hydrodynamic process study. *Journal of Physical Oceanography*, 28,
818 309-321.
819 Cacchione, D.A., P.L. Wiberg, J. Lynch, J. Irish and P. Traykovski. – 1999. Estimates of
820 suspended-sediment flux and bedform activity on the inner portion of the Eel continental shelf.
821 Mar. Geol., 154: 83-97.
822 Carlin, J. A., Dellapenna, T. M., 2014. Event-driven deltaic sedimentation on a low-gradient,
823 low-energy shelf: The Brazos River subaqueous delta, northwestern Gulf of Mexico. *Marine*
824 *Geology*, 353, 21-30.
825 Constantin, S., Constantinescu, Ș., Doxaran, D., 2017. Long-term analysis of turbidity patterns in
826 Danube Delta coastal area based on MODIS satellite data. *Journal of Marine Systems,* 170, 10-
827 21.
828 Constantinescu, Ș., Giosan, L., 2017. Marginal deltaic coasts in transition: From natural to
829 anthropogenic along the southern Romanian cliffed coast. *Anthropocene*, 19, 35-44.
830 Correggiari, A., Cattaneo, A., Trincardi, F., 2005. The modern Po Delta system: lobe switching
831 and asymmetric prodelta growth. *Marine Geology*, 222, 49-74.
832 Dalrymple, R.W. and Choi, K., 2007. Morphologic and facies trends through the fluvial–marine
833 transition in tide-dominated depositional systems: a schematic framework for environmental and
834 sequence-stratigraphic interpretation. *Earth-Science Reviews*, *81*(3-4), pp.135-174.
835 Dail, M.B., Corbett, D.R., Walsh, J.P., 2007. Assessing the importance of tropical cyclones on
836 continental margin sedimentation in the Mississippi delta region. *Continental Shelf Research*, 27,
837 1857-1874.

838 Dan, S., Stive, M. J., Walstra, D. J. R., Panin, N., 2009. Wave climate, coastal sediment budget
839 and shoreline changes for the Danube Delta. *Marine Geology*, 262, 39-49.
840 Dee, D.P., Uppala, S.M., Simmons, A.J., Berrisford, P., Poli, P., Kobayashi, S., Andrae, U.,
841 Balmaseda, M.A., Balsamo, G., Bauer, D.P. and Bechtold, P., 2011. The ERA-Interim
842 reanalysis: Configuration and performance of the data assimilation system. *Quarterly Journal of*
843 *the royal meteorological society*, *137*(656), pp.553-597.
844 DHI, Mike,2017a. MIKE 21 & MIKE 3 Flow Model, Hydrodynamic and Transport module,
845 Scientific Documentation. *Hørsholm, Denmark: DHI Water Environment Health*.
846 DHI, Mike, 2017b. MIKE 21 Spectral Wave Module, Scientific Documentation. *Hørsholm,*
847 *Denmark: DHI Water Environment Health*.
848 DHI, Mike, 2017c. MIKE 21 & MIKE 3 Flow Model FM, Sand transport module, Scientific
849 Documentation. *Hørsholm, Denmark: DHI Water Environment Health*.
850 Deigaard, R., Fredsøe, J., Hedegaard, I. B., 1986. Suspended sediment in the surf zone. *Journal*
851 *of Waterway, Port, Coastal, and Ocean Engineering*, 112, 115–128, doi:10.1061/(asce)0733-
852 950x(1986)112:1(115)
853 Dinu, I., Bajo, M., Lorenzetti, G. L., Umgiesser, G., Zaggia, L., Maximov, G., Stănica, A. S.
854 2013. Discussion concerning the current circulation along the Romanian Black Sea coast.
855 GeoEcoMarina, (19).
856 Dufois, F., Verney, R., Le Hir, P., Dumas, F., Charmasson, S., 2014. Impact of winter storms on
857 sediment erosion in the Rhône River prodelta and fate of sediment in the Gulf of Lions (North
858 Western Mediterranean Sea). *Continental Shelf Research*, 72, 57-72.
859 Dyer, K. R., 1995. Sediment transport processes in estuaries. In *Developments in*
860 *Sedimentology* (Vol. 53, pp. 423-449). Elsevier.

Eidam, E. F., Nittrouer, C. A., Ogston, A. S., DeMaster, D. J., Liu, J. P., Nguyen, T. T., Nguyen, T. N., 2017. Dynamic controls on shallow clinoform geometry: Mekong Delta, Vietnam. *Continental Shelf Research*, *147*, 165-181.

Falcini, F., Fagherazzi, S., Jerolmack, D. J., 2012. Wave-supported sediment gravity flows currents: Effects of fluid-induced pressure gradients and flow width spreading. *Continental Shelf Research*, *33*, 37-50.

Fox, J.M., Hill, P.S., Milligan, T.G., Boldrin, A., 2004a. Flocculation and sedimentation on the Po River Delta. Marine Geology 203, 95–107.

Fox, J.M., Hill, P.S., Milligan, T.G., Boldrin, A., Ogston, A., 2004b. Floc fraction in the waters of the Po River prodelta Continental Shelf Research 24 (15), 1699–1715.

Frascari, F., Spagnoli, F., Marcaccio, M., Giordano, P.,2006. Anomalous Po River flood event effects on sediments and the water column of the northwestern Adriatic Sea. *Climate Research*, *31*(2-3), 151-165.

Fraticelli, C. M., 2006. Climate forcing in a wave-dominated delta: The effects of drought–flood cycles on delta progradation. *Journal of Sedimentary Research*, *76*(9), 1067-1076.

Friedrichs, C.T., Wright, L.D., Hepworth, D.A., Kim, S.C., 2000. Bottom boundary layer processes associated with fine sediment accumulation in coastal seas and bays. Continental Shelf Research 20, 807–841.

Friedrichs, C. T., Scully, M. E., 2007. Modeling deposition by wave-supported gravity flows on the Po River prodelta: from seasonal floods to prograding clinoforms. *Continental Shelf Research*, *27*(3-4), 322-337.

882 Galloway, W.E., 1975. Process framework for describing the morphologic and stratigraphic
883 evolution of deltaic depositional systems. In: Deltas, Models for Exploration (Ed. M.L.
884 Broussard), pp. 87–98. Houston Geological Society, Houston, TX.
885 Geyer, W. R., 1993. The importance of suppression of turbulence by stratification on the
886 estuarine turbidity maximum. Estuaries, 16(1), 113-125.
887 Geyer, W.R., Hill, P.S., Kineke, G.C., 2004. The transport, transformation and dispersal of
888 sediment by buoyant coastal flows. Continental Shelf Research 24 (7–8), 927–949.
889 Geyer, W.R., Hill, P.S., Milligan, T.G., 2000. Fluid and sediment dynamics in the Eel River
890 flood plume. Continental Shelf Research 20, 2112–2120.
891 Giosan, L., Bokuniewicz, H., Panin, N., & Postolache, I., 1999. Longshore sediment transport
892 pattern along the Romanian Danube delta coast. *Journal of Coastal Research*, 859-871.
893 Guillén, J., Bourrin, F., Palanques, A., De Madron, X. D., Puig, P., & Buscail, R., 2006.
894 Sediment dynamics during wet and dry storm events on the Têt inner shelf (SW Gulf of Lions).
895 Marine Geology, 234(1-4), 129-142.
896 Halcrow,2011. Wave Modelling Report: Reduction of Coastal Erosion on the Black Sea Coast,
897 for A. N. Romanian Water Basin Administration Dobrogea – Litoral.
898 Hare, R., Eakins, B., Amante, C., 2011. Modelling bathymetric uncertainty. The International
899 Hydrographic Review, (6).
900 Harris, C. K., P. A. Traykovski, W. R. Geyer, 2005, Flood dispersal and deposition by near-bed
901 gravitational sediment flows and oceanographic transport: A numerical modeling study of the
902 Eel River shelf, northern California, J. Geophys. Res., 110, C09025, doi:10.1029/2004JC002727.
903 Harris, C. K., C. R. Sherwood, R. P. Signell, A. J. Bever, J. C. Warner, 2008. Sediment dispersal
904 in the northwestern Adriatic Sea, *J. Geophys. Res.*, **113**, C11S03, doi:10.1029/2006JC003868.

905 Hill, P.S., Milligan, T.G., Geyer, W.R., 2000. Controls on effective settling velocity of
906 suspended sediment in the Eel River flood plume. Continental Shelf Research 20, 2095–2111.
907 Hori, K., Tanabe, S., Saito, Y., Haruyama, S., Nguyen, V., & Kitamura, A., 2004. Delta initiation
908 and Holocene sea-level change: example from the Song Hong (Red River) delta,
909 Vietnam. *Sedimentary Geology*, *164*(3-4), 237-249.
910 Knauss, J.A., 1997. Introduction to Physical Oceanography, 2nd edn. Prentice Hall, Upper
911 Saddle River, NJ, 309 pp.
912 Komen, G. J., Cavaleri, L., Donelan, M., Hasselmann, K., Hasselmann, S., Janssen, P. A. E. M.,
913 1996. Dynamics and modelling of ocean waves. pp. 554. ISBN 0521577810. Cambridge, UK:
914 Cambridge University Press.
915 Kranck, K., 1980. Experiments on the significance of flocculation in the settling behaviour of
916 fine grained sediment in still water. Canadian Journal Earth Science 17, 1517–1526.
917 Lentz, S.J., 2001. The influence of stratification on the wind-driven cross-shelf circulation over
918 the north Carolina shelf. J. Phys. Oceanogr. 23, 2749–2760.
919 Liu, J. P., Xu, K. H., Li, A. E. A., Milliman, J. D., Velozzi, D. M., Xiao, S. B., Yang, Z. S., 2007.
920 Flux and fate of Yangtze River sediment delivered to the East China Sea. Geomorphology, 85(3-
921 4), 208-224.
922 Ma, Y., Wright, L.D., Friedrichs, C.T., 2008. Observations of sediment transport on the
923 continental shelf off the mouth of the Waiapu River, New Zealand: evidence for current
924 supported gravity flows. Continental Shelf Research 28 (4–5), 516–532.Maillet, G. M., Vella, C.,
925 Berné, S., Friend, P. L., Amos, C. L., Fleury, T. J., Normand, A., 2006. Morphological changes
926 and sedimentary processes induced by the December 2003 flood event at the present mouth of
927 the Grand Rhône River (southern France). *Marine Geology*, *234*(1-4), 159-177.

928 Malagó, A., Bouraoui, F., Vigiak, O., Grizzetti, B., Pastori, M., 2017. Modelling water and
929 nutrient fluxes in the Danube River Basin with SWAT. *Science of the Total Environment*, *603*,
930 196-218.
931 Marion, C., Dufois, F., Arnaud, M., Vella, C., 2010. In situ record of sedimentary processes near
932 the Rhône River mouth during winter events (Gulf of Lions, Mediterranean Sea). Continental
933 Shelf Research, 30(9), 1095–1107. doi:10.1016/j.csr.2010.02.015
934 Mil-Homens, J., Ranasinghe, R., Van Thiel de Vries, J.S.M., Stive, M.J.F., 2013. Re-evaluation
935 and improvement of three commonly used bulk longshore sediment transport formulas. Coastal
936 Engineering 75, 29-39
937 Milligan, T. G., Hill, P. S., Law, B. A., 2007. Flocculation and the loss of sediment from the Po
938 River plume. *Continental Shelf Research*, *27*(3-4), 309-321.
939 Milliman, J.D., Quraishee, G.S., Beg, M.A.A., 1984. Sediment discharge from the Indus River to
940 the ocean: past, present and future. In: Haq, B.U., Milliman, J.D. (Eds.), Marine Geology and
941 Oceanography of Arabian Sea and Coastal Pakistan. Van Nostrand Reinhold, New York, pp. 65–
942 70.
943 Milliman, J.D. and Syvitski, J.P., 1992. Geomorphic/tectonic control of sediment discharge to
944 the ocean: the importance of small mountainous rivers. *The journal of Geology*, *100*(5), pp.525-
945 544.
946 Moritz H., Moritz H., 2006. Evaluating extreme storm power and potential implications to
947 coastal infras-tructure damage. In: 9th International workshop on wave hindcasting and
948 forecasting, Oregon Coast, USA.
949 Nienhuis, J. H., Ashton, A. D., Giosan, L., 2015. What makes a delta wave-dominated? Geology,
950 43(6), 511-514. 2015.

951 Nienhuis, J. H., Ashton, A. D., Roos, P. C., Hulscher, S. J., Giosan, L., 2013. Wave reworking of
952 abandoned deltas. Geophysical research letters,40(22), 5899-5903.
953 Nittrouer, C.A., 1999. STRATAFORM: overview of its design and synthesis of its results.
954 Marine Geology 154, 3–12
955 Nittrouer, C.A., Miserocchi, S., Trincardi, F., 2004. The PASTA project: investigation of Po and
956 Apennine sediment transport and accumulation. Oceanography 17 (4), 46–57.
957 Nowacki, D. J., Horner-Devine, A. R., Nash, J. D., Jay, D. A., 2012. Rapid sediment removal
958 from the Columbia River plume near field. Continental Shelf Research, 35, 16-28.
959 Pinto L., Fortunato A.B., Freire P., 2006. Sensitivity analysis of non-cohesive sediment transport
960 formulae. Continental Shelf Research, 26, 1826-1839.
961 Ogston, A.S., Sternberg R.W., 1999. Sediment-transport events on the northern California
962 continental shelf. Mar. Geol., 154: 69-82.
963 Poggioli, A., Horner-Devine, A., 2018. Two-layer hydraulics at the river–ocean interface.
964 Journal of Fluid Mechanics, 856, 633-672. doi:10.1017/jfm.2018.688
965 Pratson, L.F., Nittrouer, C.A., Wiberg, P.L., Steckler, M.S., Swenson, J.B., Cacchione, D.A.,
966 Karson, J.A., Murray, A.B., Wolinsky, M.A., Gerber, T.P. and Mullenbach, B.L., 2007. Seascape
967 evolution on clastic continental shelves and slopes. *Continental margin sedimentation: from*
968 *sediment transport to sequence stratigraphy*, pp.339-380.
969 Preoteasa, L., Vespremeanu-Stroe, A., Tătui, F., Zăinescu, F., Timar-Gabor, A., Cîrdan, I., 2016.
970 The evolution of an asymmetric deltaic lobe (Sf. Gheorghe, Danube) in association with cyclic
971 development of the river-mouth bar: Long-term pattern and present adaptations to human-
972 induced sediment depletion. Geomorphology, 253, 59-73,

973 Provansal, M., Pichard, G., Anthony, E.J., 2015. Geomorphic changes in the Rhône delta during
974 the LIA: input from the analysis of ancient maps. In: Robin, M, Maanan, M (Eds.), Coastal
975 Sediment Fluxes. Coastal Research Library, pp. 47–72.
976 Rodriguez, A. B., Hamilton, M. D., & Anderson, J. B.,2000. Facies and Evolution of the Modern
977 Brazos Delta, Texas: Wave Versus Flood Influence. Journal of Sedimentary Research, 70(2),
978 283–295. doi:10.1306/2dc40911-0e47-11d7-8643000102c1865d
979 Ruessink, B. G., Walstra, D. J. R., & Southgate, H. N., 2003. Calibration and verification of a
980 parametric wave model on barred beaches. *Coastal Engineering*, *48*(3), 139-149.
981 Rusu, L., Bernardino, M., Guedes Soares, C., 2014. Wind and wave modelling in the Black Sea.
982 Journal of Operational Oceanography, 7(1), 5-20.
983 Rusu, L., 2015. Assessment of the wave energy in the Black Sea based on a 15-year hindcast
984 with data assimilation. *Energies*, *8*(9), 10370-10388.
985 Sabatier, F., Maillet, G., Provansal, M., Fleury, T. J., Suanez, S., Vella, C., 2006. Sediment
986 budget of the Rhône delta shoreface since the middle of the 19th century. *Marine*
987 *Geology*, *234*(1-4), 143-157.Schubel, J. R., Carter, H. H., 1984. The estuary as a filter for fine-
988 grained suspended sediment. In *The estuary as a filter* (pp. 81-105).
989 Sha, X., Xu, K., Bentley, S. J., Robichaux, P. A., 2018. Characterization and modeling of
990 sediment settling, consolidation, and suspension to optimize coastal Louisiana
991 restoration. *Estuarine, Coastal and Shelf Science*, *203*, 137-147.
992 Shore Protection Manual, 1984. U.S. Army Corps of Engineers, Coastal Engineering Research
993 Center, U.S. Government Printing Office, Washington, D.C.
994 Stănescu, V., 1967. Dunarea intre Bazias si Ceatal Izmail. Monografie hidrologica. Editura
995 tehnica. Bucuresti, 1967, p.1-372.

996 Stanley, D.J., Warne, A.G., 1994. Worldwide initiation of holocene marine deltas by
997 deceleration of sea-level rise. Science 265, 228–231.
998 Syvitski, J.P. and Saito, Y., 2007. Morphodynamics of deltas under the influence of
999 humans. *Global and Planetary Change*, *57*(3-4), pp.261-282.
1000 Szczuciński, W., Jagodziński, R., Hanebuth, T.J., Stattegger, K., Wetzel, A., Mitręga, M.,
1001 Unverricht, D., Van Phach, P., 2013. Modern sedimentation and sediment dispersal pattern on
1002 the continental shelf off the Mekong River delta, South China Sea. *Global and planetary*
1003 *change*, *110*, pp.195-213.
1004 Ta, T. K. O., Nguyen, V. L., Tateishi, M., Kobayashi, I., Tanabe, S., Saito, Y., 2002. Holocene
1005 delta evolution and sediment discharge of the Mekong River, southern Vietnam. *Quaternary*
1006 *Science Reviews*, *21*(16-17), 1807-1819.
1007 Tamura, T., Saito, Y., Sieng, S., Ben, B., Kong, M., Sim, I., Choup, S. and Akiba, F., 2009.
1008 Initiation of the Mekong River delta at 8 ka: evidence from the sedimentary succession in the
1009 Cambodian lowland. *Quaternary Science Reviews*, *28*(3-4), pp.327-344.
1010 Tătui, F., Vespremeanu-Stroe, A., Ruessink, G. B., 2016. Alongshore variability of cross-shore
1011 bar behavior on a nontidal beach. *Earth Surface Processes and Landforms*, *41*(14), 2085-2097.
1012 Tătui, F., Vespremeanu-Stroe, A., 2017. Evolution and morphodynamics of Danube Delta
1013 shoreface. In *Landform Dynamics and Evolution in Romania* (pp. 607-626). Springer, Cham.
1014 Tesi, T., Miserocchi, S., Goñi, M. A., Turchetto, M., Langone, L., De Lazzari, A., ... Correggiari,
1015 A., 2011. Influence of distributary channels on sediment and organic matter supply in event-
1016 dominated coastal margins: the Po prodelta as a study case. *Biogeosciences*, *8*(2), 365.

1017 Thanh, V. *Q*., Reyns, J., Wackerman, C., Eidam, E. F., Roelvink, D., 2017. Modelling suspended
1018 sediment dynamics on the subaqueous delta of the Mekong River. *Continental Shelf*
1019 *Research*, *147*, 213-230.
1020 Traykovski, P., Geyer, W.R., Irish, J.D., Lynch, J.F., 2000. The role of wave-induced density-
1021 driven fluid mud flows for cross-shelf transport on the Eel River continental shelf. *Continental*
1022 *Shelf Research*, *20*(16), pp.2113-2140.
1023 van Gils J., Schwanenberg D., van Kessel T., Walstra D., 2006. Deep Water Navigation Canal
1024 Danube Black Sea. Report by Delft Hydraulics to the ESPOO Inquiry Commission.
1025 van Maren, D. S., & Hoekstra, P., 2005. Dispersal of suspended sediments in the turbid and
1026 highly stratified Red River plume. Continental Shelf Research, 25(4), 503-519.
1027 van Rijn, L.C., 1984. Sediment Transport, Part II: Suspended Load Transport. Journal of
1028 Hydraulic Engineering, ASCE, Vol. 110, No. 11.
1029 van Rijn, L. C., 2014. A simple general expression for longshore transport of sand, gravel and
1030 shingle. *Coastal Engineering*, *90*, 23-39.
1031 Vanoni, V. A., 1964. Measurements of critical shear stress for entraining fine sediments in a
1032 boundary layer.
1033 Vespremeanu E., 1983. Geomorphological evolution of Sfântu Gheorghe arm mouth (Danube
1034 Delta, North-West of the Black Sea) in the last 200 years. Rev. Roum Geol., Geophys., Geogr.,
1035 Tome 27, p. 61-68, Bucuresti.
1036 Vespremeanu-Stroe, A., 2004. Transportul de sedimente în lungul ţărmului şi regimul valurilor
1037 pe coasta Deltei Dunării. Studii şi cercetări de oceanografie costieră, 1, 67-82.

1038 Vespremeanu-Stroe, A., Constantinescu, Ş., Tătui, F., Giosan, L., 2007. Multi-decadal evolution
1039 and North Atlantic Oscillation influences on the dynamics of the Danube Delta
1040 shoreline. *Journal of Coastal Research*, 157-162.
1041 Vespremeanu-Stroe, A., Zăinescu, F., Preoteasa, L., Tătui, F., Rotaru, S., Morhange, C., Stoica,
1042 M., Hanganu, J., Timar-Gabor, A., Cârdan, I., Piotrowska, N.,2017. Holocene evolution of the
1043 Danube delta: An integral reconstruction and a revised chronology. *Marine Geology*, *388*, 38-61.
1044 Vörösmarty, C.J., Meybeck, M., Fekete, B., Sharma, K., Green, P. Syvitski, J.P., 2003.
1045 Anthropogenic sediment retention: major global impact from registered river
1046 impoundments. *Global and planetary change*, *39*(1-2), pp.169-190.Walsh, J. P., Nittrouer, C. A.,
1047 2009. Understanding fine-grained river-sediment dispersal on continental margins. *Marine*
1048 *Geology*, *263*(1-4), 34-45.
1049 Warrick, J. A., 2014. Eel River margin source-to-sink sediment budgets: Revisited. *Marine*
1050 *Geology*, *351*, 25-37.
1051 Weatherall, P., Marks, K. M., Jakobsson, M., Schmitt, T., Tani, S., Arndt, J. E., Rovere, M.,
1052 Chayes, D., Ferrini, V., Wigley, R., 2015. A new digital bathymetric model of the world's
1053 oceans. *Earth and Space Science*, *2*(8), 331-345.
1054 Winterwerp, J.C., van Kesteren, W.G.M., 2004. Introduction to the Physics of Cohesive
1055 Sediment in the Marine Environment: Developments in Sedimentology. volume 56 Elsevier,
1056 Amsterdam, The Netherlands.
1057 Wright L.D., 1985. River Deltas. In: Davis, R.A. (ed.), Coastal Sedimentary Environments.
1058 Springer-Verlag, New York, pp. 1-76.
1059 Wright, L.D.,Coleman, J.M., 1973. Variations in morphology of major river deltas as functions
1060 of ocean wave and river discharge regimes. AAPG Bull., 57, 370–398, 1973.

1061 Wright, L.D., Nittrouer, C.A., 1995. Dispersal of river sediments in coastal seas: six contrasting
1062 cases. *Estuaries*, *18*(3), pp.494-508.
1063 Wright, L.D., Kim S.C., Friedrichs C.T., 1999. Across-shelf variations in bed roughness, bed
1064 stress and sediment suspension on the northern California shelf. Mar. Geol., 154: 99-115
1065 Wright, L.D., Friedrichs, C.T., 2006. Gravity-driven sediment transport on continental shelves: A
1066 status report. Continental Shelf Research 26, 2092-2107.
1067 Xu, K., Corbett, D. R., Walsh, J. P., Young, D., Briggs, K. B., Cartwright, G. M., Friedrichs,
1068 C.T., Harris, C.K., Mickey, R.C., Mitra, S., 2014. Seabed erodibility variations on the Louisiana
1069 continental shelf before and after the 2011 Mississippi River flood. *Estuarine, Coastal and Shelf*
1070 *Science*, *149*, 283-293.
1071 Xue, Z., Liu, J., Demaster, D., Nguyen, V., Oanh Ta, T.K., 2010. Late Holocene Evolution of the
1072 Mekong Subaqueous Delta, Southern Vietnam. Marine Geology 269(1-2), 46-60
1073 Zăinescu, F. I., Tătui, F., Valchev, N. N., Vespremeanu-Stroe, A., 2017. Storm climate on the
1074 Danube delta coast: evidence of recent storminess change and links with large-scale
1075 teleconnection patterns. Natural Hazards, 87 (2), 599-621.
1076 Zăinescu, F. I., Vespremeanu-Stroe, A., Tătui, F., Preoteasa, L., Anthony, E.J., 2018. Flood
1077 deposition and storm resuspension of sediments in front of a deltaic wave-influenced river
1078 mouth: Insights from 14 years of measurements and numerical modelling. EGU General
1079 Assembly Conference Abstracts (Vol. 20, p. 16617).
1080
1081 **Figure and table captions**
1082
1083 Table 1. Discharge and storm percentiles used throughout the paper and their corresponding
1084 thresholds. *Q* for Sf. Gheorghe is ~¼ of the total Danube *Q*.

Figure 1. The Danube River basin and the Black Sea (A), Danube delta, location of study area, and the data used throughout the paper (B). The Danubian Current is shown in relation to north (downwelling, blue) and south (upwelling, red) winds. Wave rose from ERA5data.

Figure 2. Sf. Gheorghe river-mouth bathymetry (A), the areas retained for the sediment volume calculations (delimited by dashed lines). Grain-size distribution (D50) in the river mouth area in July 2005 and a selection of shallow cores from 2004 (B). Monthly discharge and wave climate (C).

Figure 3. Frequency of discharge and wave height (top) in hours/yr. Frequency of wave height and direction (down). Era Interim data.

Figure 4. Meshes used for Mike modelling.

Figure 5. Comparison of measured data and model results: current velocity (A); current direction (B), for the ADCP transect shown in fig. 2; wave heights (C).

Figure 6. Spectrum of bathymetric change and selected bathymetric differences illustrating extreme, intermediate, and low change. T_{05} to T_{18} represent the time intervals between bathymetric differences, T_{05} = 2004 : 2005.

Figure 7. Time series of liquid discharge *Q* (red line), solid discharge *Qs* (red bars) (A); 6-hourly offshore *Hs* and cumulative storm power for each period (B); duration of selected flood and storm percentiles; note that each percentile has its own scale (C); volume changes for each of the areas shown in Fig. 2. (D); positive, negative and net volume changes (E). T_{05} to T_{18} represent the time intervals between bathymetric differences

Figure 8. Scatter plots of volume change (ΔV) and FL/ST_i for the whole river mouth area (ΔV Total), left plots; only for the crest area (ΔV Crest), right plots; FL/ST_{dur} based on duration proxies (top); FL/ST_{sed} based on wave power and sediment discharge proxies (bottom). The blue area shows the 95% confidence interval for the linear fit.

Figure 9. Results of flood simulations for different thresholds. Surface velocity fields (A), vertical fields of velocity at 4972000 latitude (B), vertical fields of salinity at 497200 latitude (C), current bed shear stress (D).

Figure 10. Results of storm simulations for different thresholds. Surface velocity fields (A), vertical velocity fields at 4972000 latitude (B), significant wave height (*Hs*) (C), combined current and wave bed shear stress (D).

Figure 11. Conceptual hydro-morphodynamic model for the river-mouth area during extreme conditions: floods (A), storms (B).

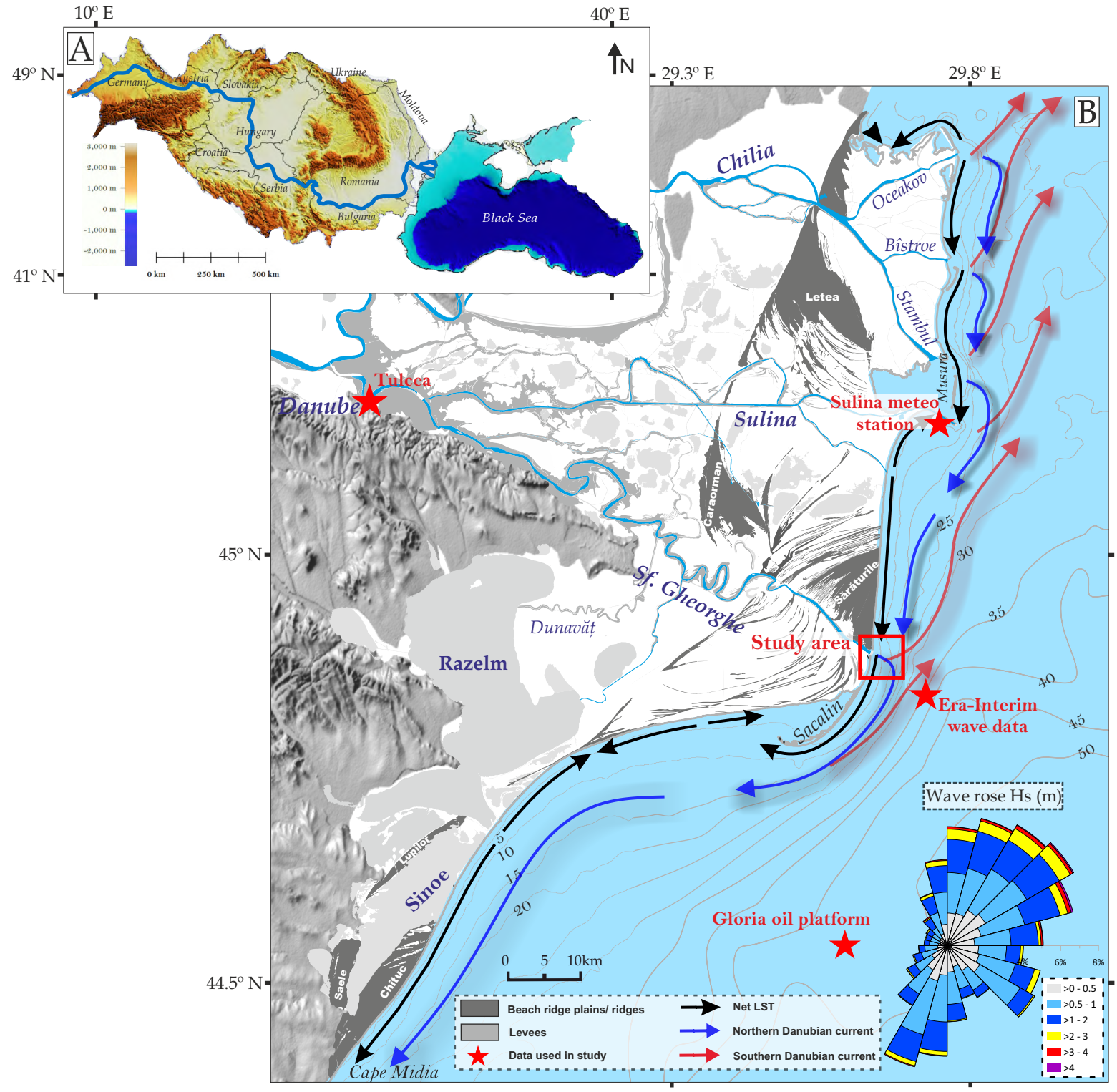
10° E
40° E
49° N
41° N
29.3° E
29.8° E
45° N
44.5° N
A
B
N
Germany
Austria
Slovakia
Ukraine
Moldova
Hungary
Croatia
Serbia
Romania
Bulgaria
Black Sea
3,000 m
2,000 m
1,000 m
0 m
-1,000 m
-2,000 m
0 km
250 km
500 km
Chilia
Oceakov
Bîstroe
Letea
Stambul
Musura
Tulcea
Danube
Sulina
Sulina meteo station
Caraorman
Sf. Gheorghe
Sărăturile
Dunavăț
Study area
Razelm
Era-Interim wave data
Sacalin
Lupilor
Sinoe
Saele
Chituc
Gloria oil platform
Cape Midia
25
30
35
40
45
50
5
10
15
20
0 5 10km
Wave rose Hs (m)
4%
6%
8%
>0 - 0.5
>0.5 - 1
>1 - 2
>2 - 3
>3 - 4
>4
Beach ridge plains/ ridges
Levees
Data used in study
Net LST
Northern Danubian current
Southern Danubian current

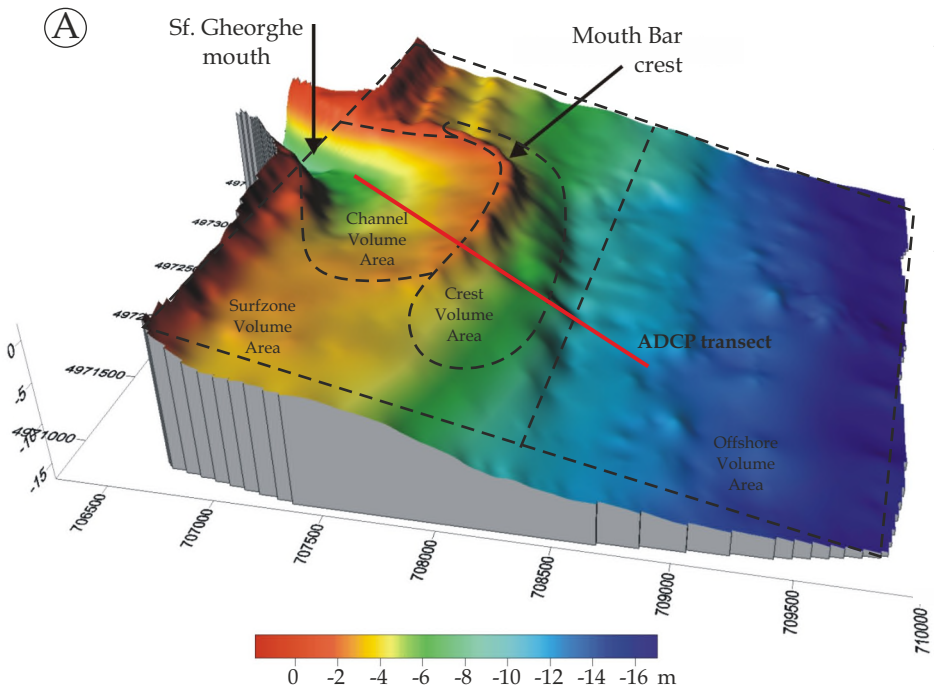
A
Sf. Gheorghe mouth
Mouth Bar crest
Channel Volume Area
Crest Volume Area
Surfzone Volume Area
Offshore Volume Area
ADCP transect
0 -2 -4 -6 -8 -10 -12 -14 -16 m

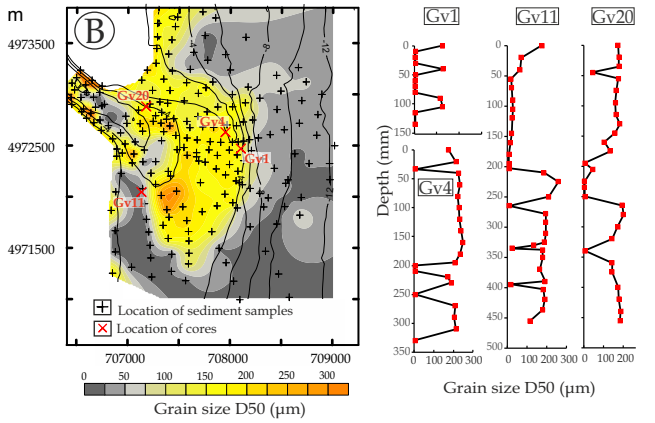
m
B
Gv20
Gv4
Gv1
Gv11
Location of sediment samples
Location of cores
Grain size D50 (μm)
Gv1
Gv11
Gv20
Gv4
Depth (mm)
Grain size D50 (μm)

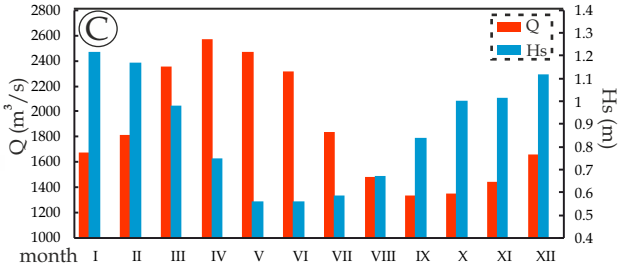
C
Q
Hs
Q (m3/s)
Hs (m)
month I II III IV V VI VII VIII IX X XI XII

Q (m^3/s)													
750	35	381	219	85	42	23	10	4	0.9	2	1		Hours/yr
1250	161	1392	733	282	130	70	37	15	12	2			
1750	109	1026	566	266	109	45	17	11	6	1	0.5	0.5	1
2250	70	602	378	184	81	32	14	5	0.5				
2750	58	413	188	68	16	4	2	0.5					
3250	27	245	121	42	22	12	5	2					
3750	29	204	57	16	5	3	0.5	1					
>4000	13	29	11	7	0.9								
Hs (m)	Calm	0.5	1	1.5	2	2.5	3	3.5	4	4.5	5	5.5	≥6

Dir (°)													
0	34	290	195	86	42	21	7	3	1				Hours/yr
22.5	43	412	222	116	59	25	16	5	1	2			
45	41	429	228	111	72	41	19	7	5				
67.5	48	390	226	121	54	25	17	12	8	3	1	0.5	1
90	31	332	153	66	26	9	4	5	2				
112.5	37	362	134	46	22	10	1	1					
135	29	270	97	19	4	3							
157.5	30	192	92	22	7	2							
180	31	250	151	42	11	5	2						
202.5	30	351	202	78	24	12	6	1	0.5				
N vs S	1.055	1.067	1.29	2.091	3.373	3.662	5.955	11.8	35				
Hs (m)	Calm	0.5	1	1.5	2	2.5	3	3.5	4	4.5	5	5.5	≥6

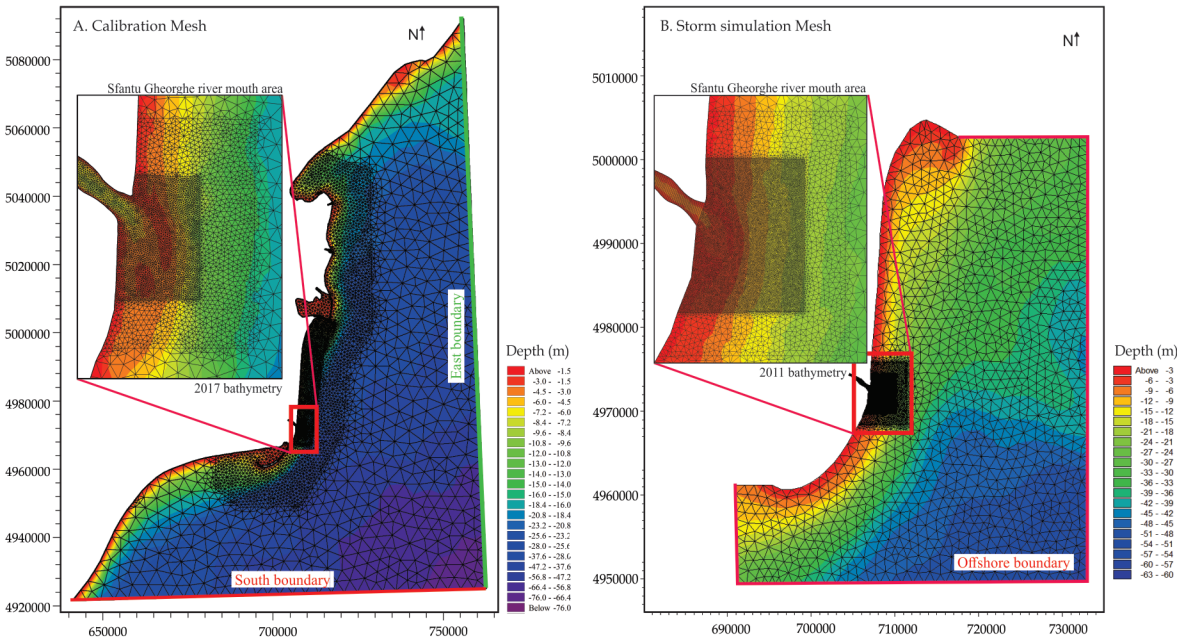
A. Calibration Mesh
N
Sfantu Gheorghe river mouth area
2017 bathymetry
East boundary
South boundary
5080000
5060000
5040000
5020000
5000000
4980000
4960000
4940000
4920000
650000
700000
750000
Depth (m)
Above -1.5
-3.0 - -1.5
-4.5 - -3.0
-6.0 - -4.5
-7.2 - -6.0
-8.4 - -7.2
-9.6 - -8.4
-10.8 - -9.6
-12.0 - -10.8
-13.0 - -12.0
-14.0 - -13.0
-15.0 - -14.0
-16.0 - -15.0
-18.4 - -16.0
-20.8 - -18.4
-23.2 - -20.8
-25.6 - -23.2
-28.0 - -25.6
-37.6 - -28.6
-47.2 - -37.6
-56.8 - -47.2
-66.4 - -56.8
-76.0 - -66.4
Below -76.0
B. Storm simulation Mesh
N
Sfantu Gheorghe river mouth area
2011 bathymetry
Offshore boundary
5010000
5000000
4990000
4980000
4970000
4960000
4950000
690000
700000
710000
720000
730000
Depth (m)
Above -3
-6 - -3
-9 - -6
-12 - -9
-15 - -12
-18 - -15
-21 - -18
-24 - -21
-27 - -24
-30 - -27
-33 - -30
-36 - -33
-39 - -36
-42 - -39
-45 - -42
-48 - -45
-51 - -48
-54 - -51
-57 - -54
-60 - -57
-63 - -60

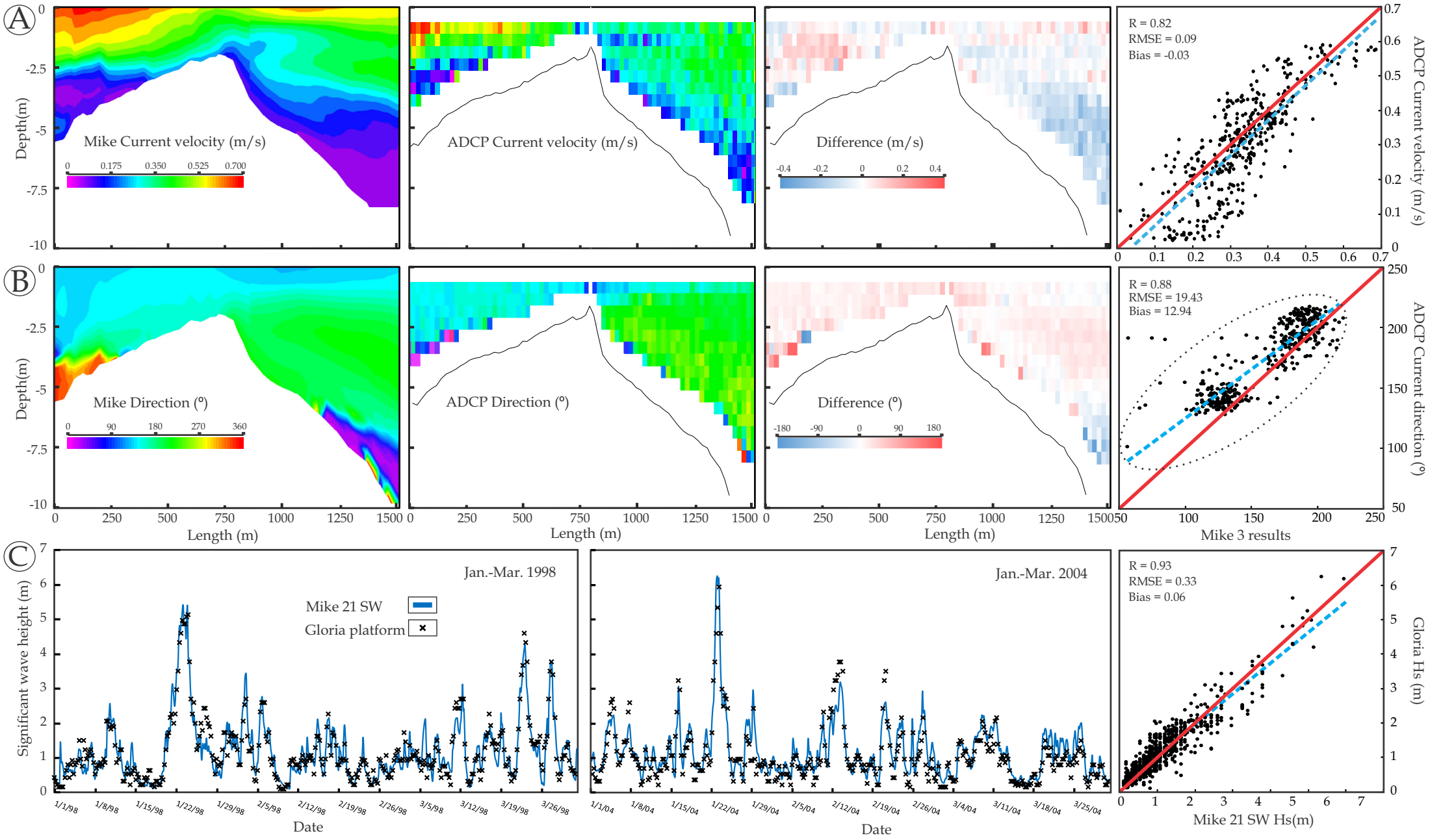
A
Depth(m)
Mike Current velocity (m/s)
ADCP Current velocity (m/s)
Difference (m/s)
R = 0.82
RMSE = 0.09
Bias = -0.03
ADCP Current velocity (m/s)
B
Mike Direction (°)
ADCP Direction (°)
Difference (°)
R = 0.88
RMSE = 19.43
Bias = 12.94
ADCP Current direction (°)
Length (m)
Mike 3 results
C
Jan.-Mar. 1998
Jan.-Mar. 2004
Mike 21 SW
Gloria platform
Significant wave height (m)
Date
R = 0.93
RMSE = 0.33
Bias = 0.06
Gloria Hs (m)
Mike 21 SW Hs(m)

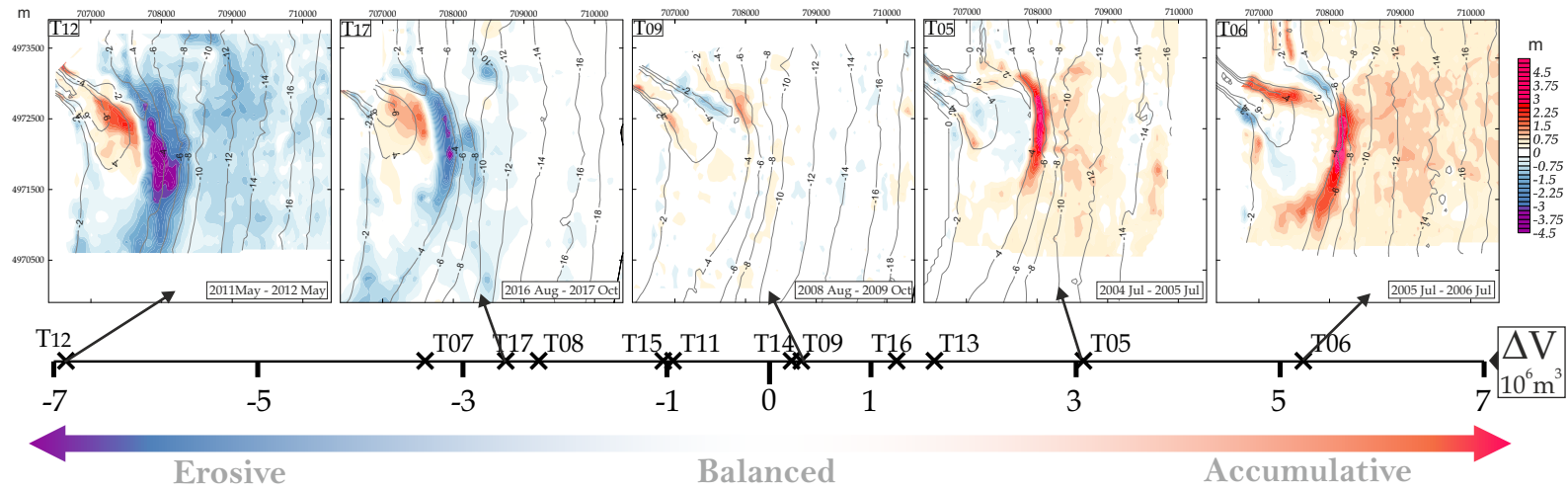
m
T12
T17
T09
T05
T06
2011May - 2012 May
2016 Aug - 2017 Oct
2008 Aug - 2009 Oct
2004 Jul - 2005 Jul
2005 Jul - 2006 Jul
4.5
3.75
3
2.25
1.5
0.75
0
-0.75
-1.5
-2.25
-3
-3.75
-4.5

T12
T07
T17
T08
T15
T11
T14
T09
T16
T13
T05
T06
ΔV
10^6 m^3
-7
-5
-3
-1
0
1
3
5
7
Erosive
Balanced
Accumulative

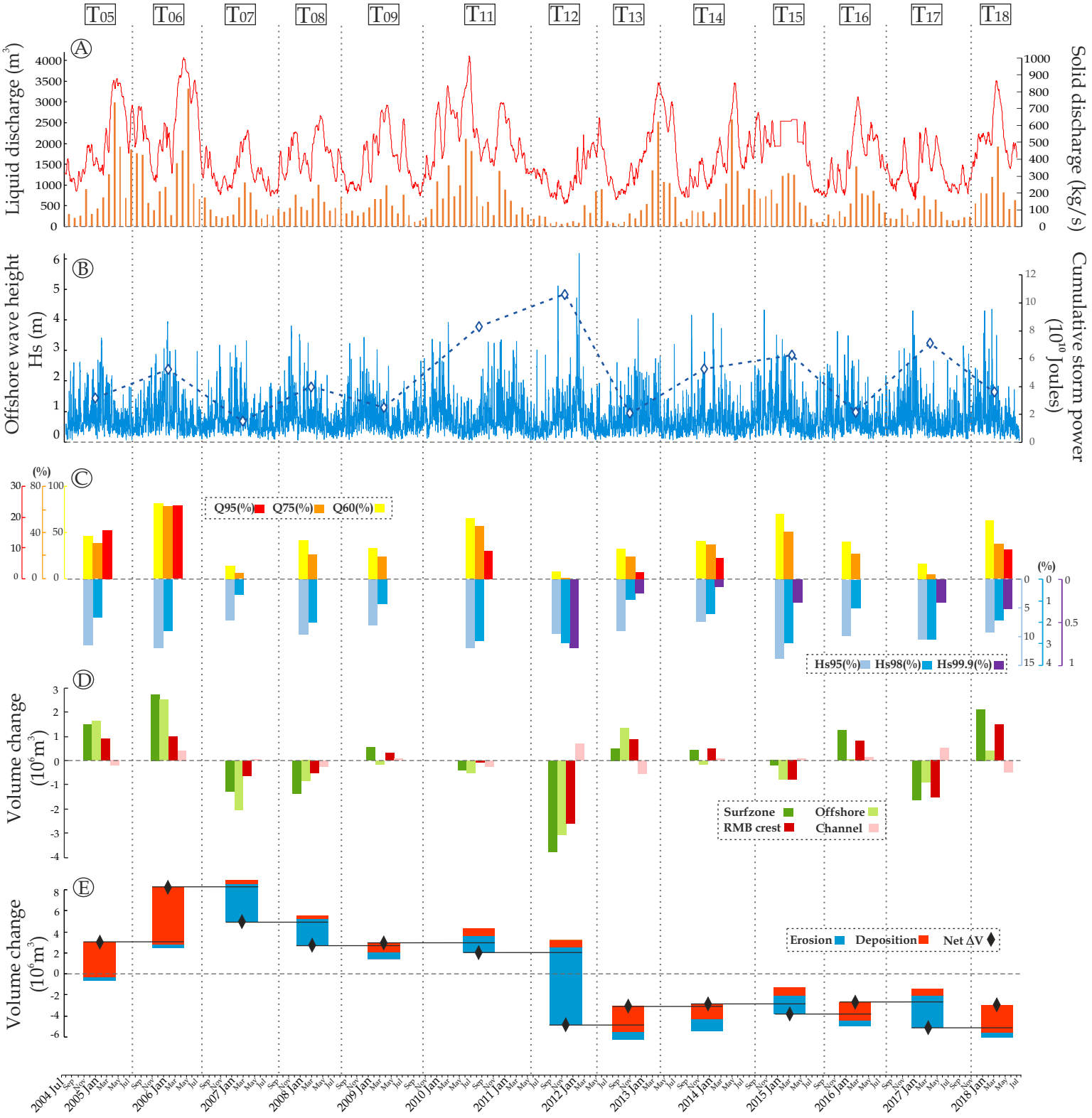
T05
T06
T07
T08
T09
T11
T12
T13
T14
T15
T16
T17
T18
A
Liquid discharge (m3)
Solid discharge (kg/s)
B
Offshore wave height Hs (m)
Cumulative storm power (10^10 Joules)
C
(%)
Q95(%) Q75(%) Q60(%)
Hs95(%) Hs98(%) Hs99.9(%)
D
Volume change (10^6 m^3)
Surfzone
Offshore
RMB crest
Channel
E
Volume change (10^6 m^3)
Erosion
Deposition
Net ΔV
2004 Jul
2005 Jan
2006 Jan
2007 Jan
2008 Jan
2009 Jan
2010 Jan
2011 Jan
2012 Jan
2013 Jan
2014 Jan
2015 Jan
2016 Jan
2017 Jan
2018 Jan

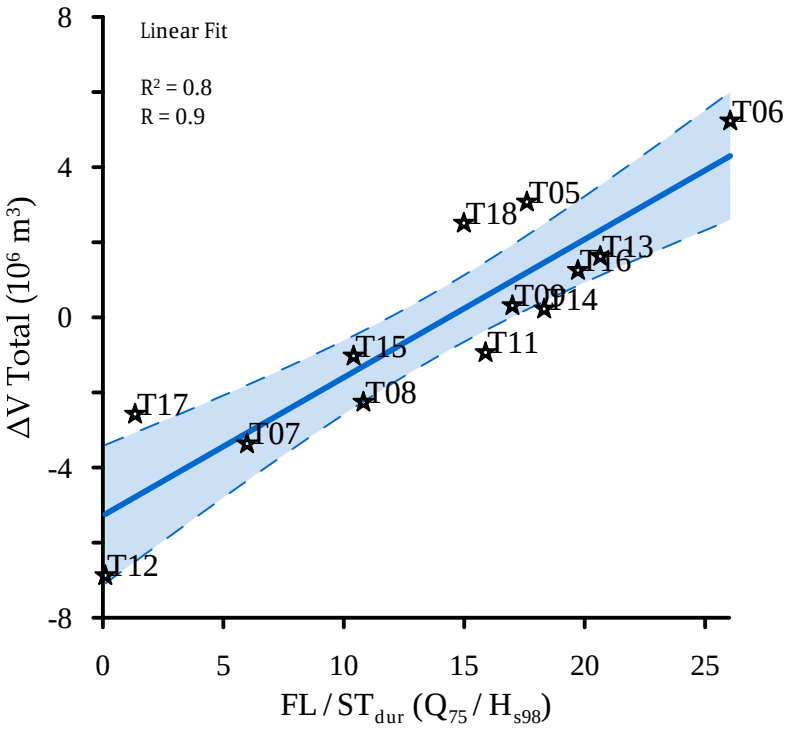
Linear Fit
R² = 0.8
R = 0.9
ΔV Total (10⁶ m³)
FL / ST_dur (Q75 / Hs98)
T06
T18
T05
T13
T16
T09
T14
T15
T11
T17
T08
T07
T12

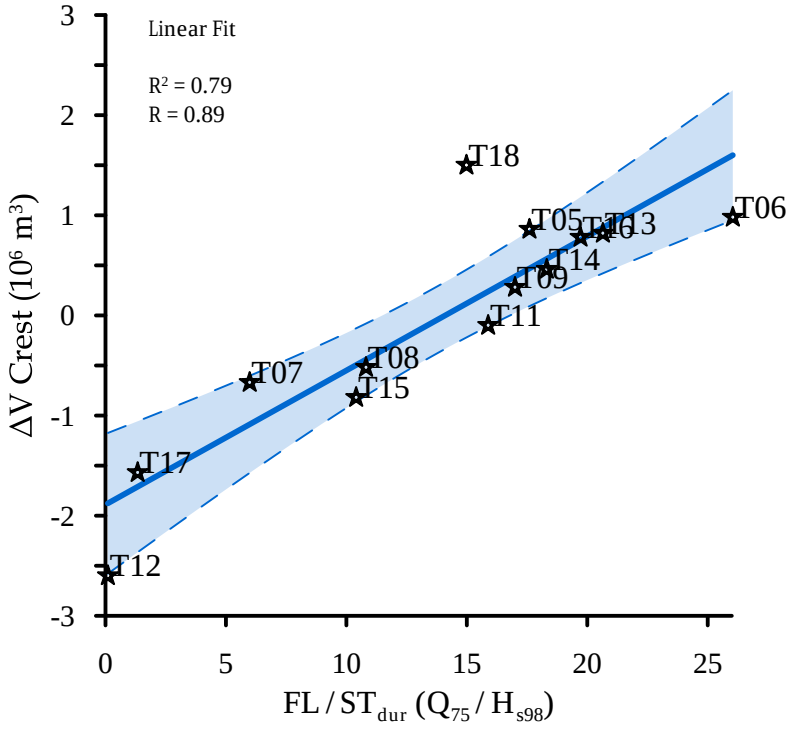
Linear Fit
R² = 0.79
R = 0.89
ΔV Crest (10⁶ m³)
FL / ST_dur (Q75 / Hs98)
T18
T06
T05
T13
T16
T14
T09
T11
T08
T07
T15
T17
T12

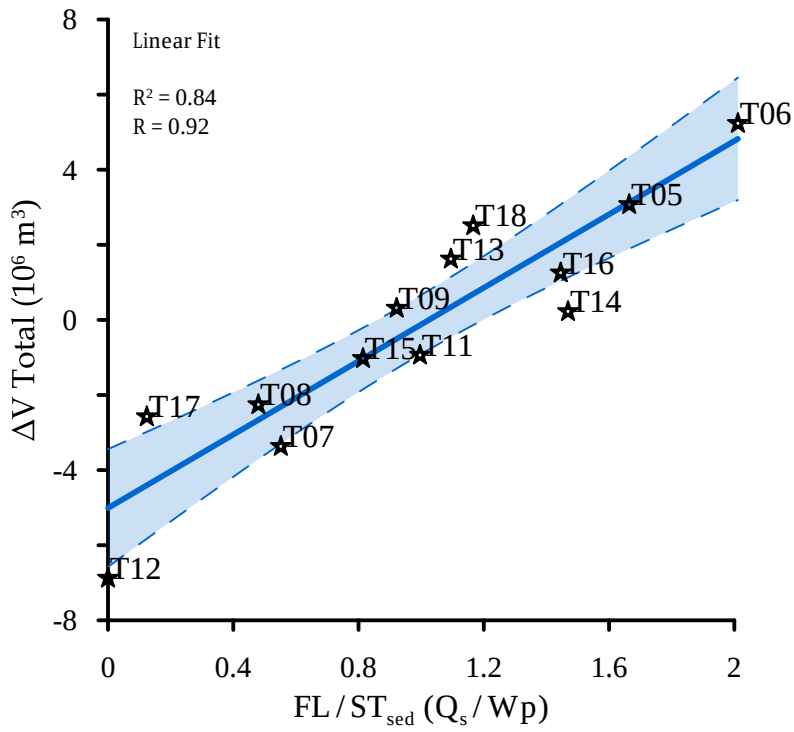
Linear Fit
R² = 0.84
R = 0.92
ΔV Total (10⁶ m³)
FL / ST_sed (Qs / Wp)
T06
T05
T18
T13
T16
T09
T14
T15
T11
T17
T08
T07
T12

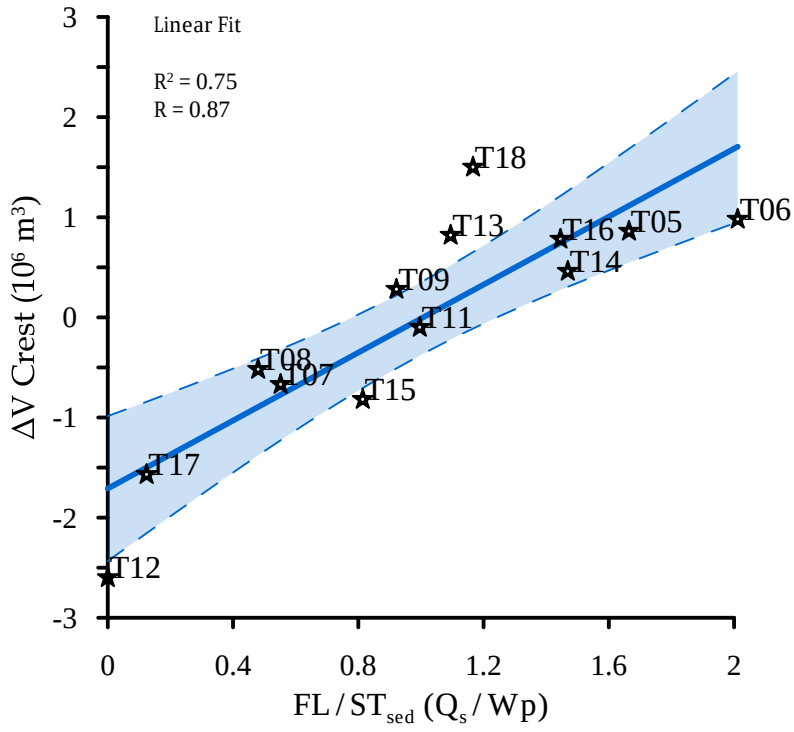
Linear Fit
R² = 0.75
R = 0.87
ΔV Crest (10⁶ m³)
FL / ST_sed (Qs / Wp)
T18
T06
T13
T16
T05
T14
T09
T11
T08
T07
T15
T17
T12

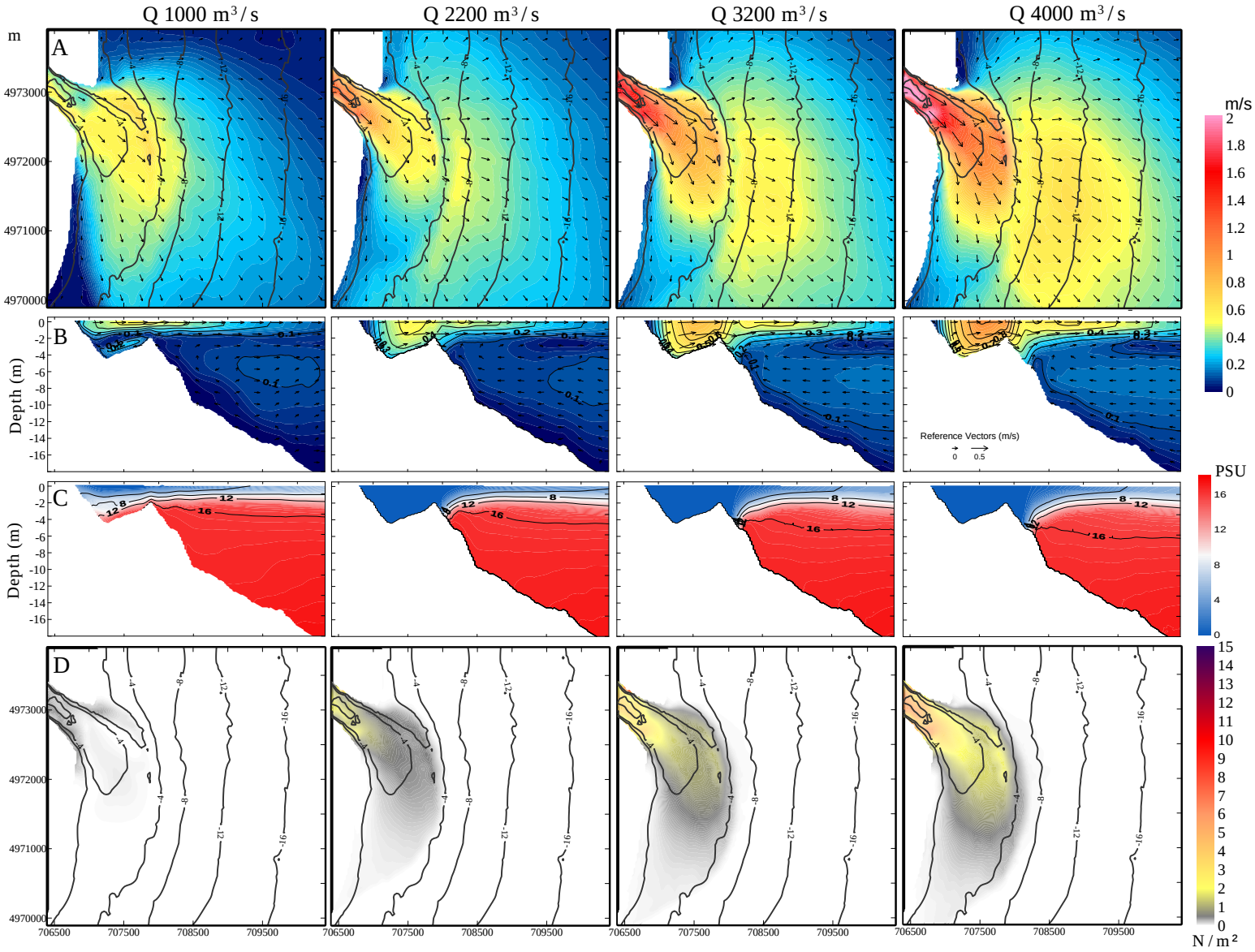
Q 1000 m³/s
Q 2200 m³/s
Q 3200 m³/s
Q 4000 m³/s
m
A
B
C
D
Depth (m)
Depth (m)
Reference Vectors (m/s)
m/s
PSU
N / m²
4973000
4972000
4971000
4970000
706500
707500
708500
709500

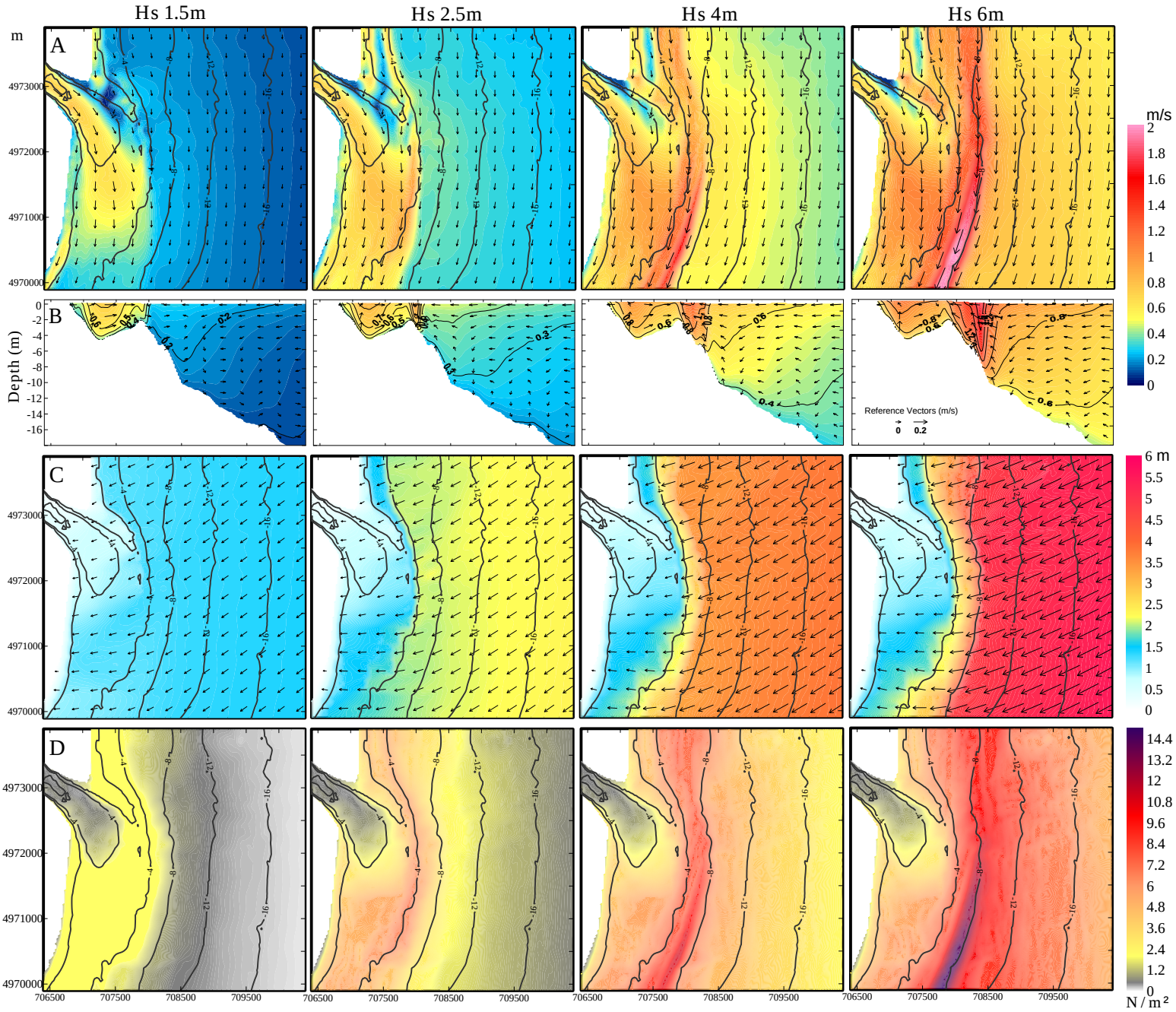
Hs 1.5m
Hs 2.5m
Hs 4m
Hs 6m
m
A
B
C
D
Depth (m)
Reference Vectors (m/s)
0
0.2
m/s
6 m
N / m²
4973000
4972000
4971000
4970000
706500
707500
708500
709500

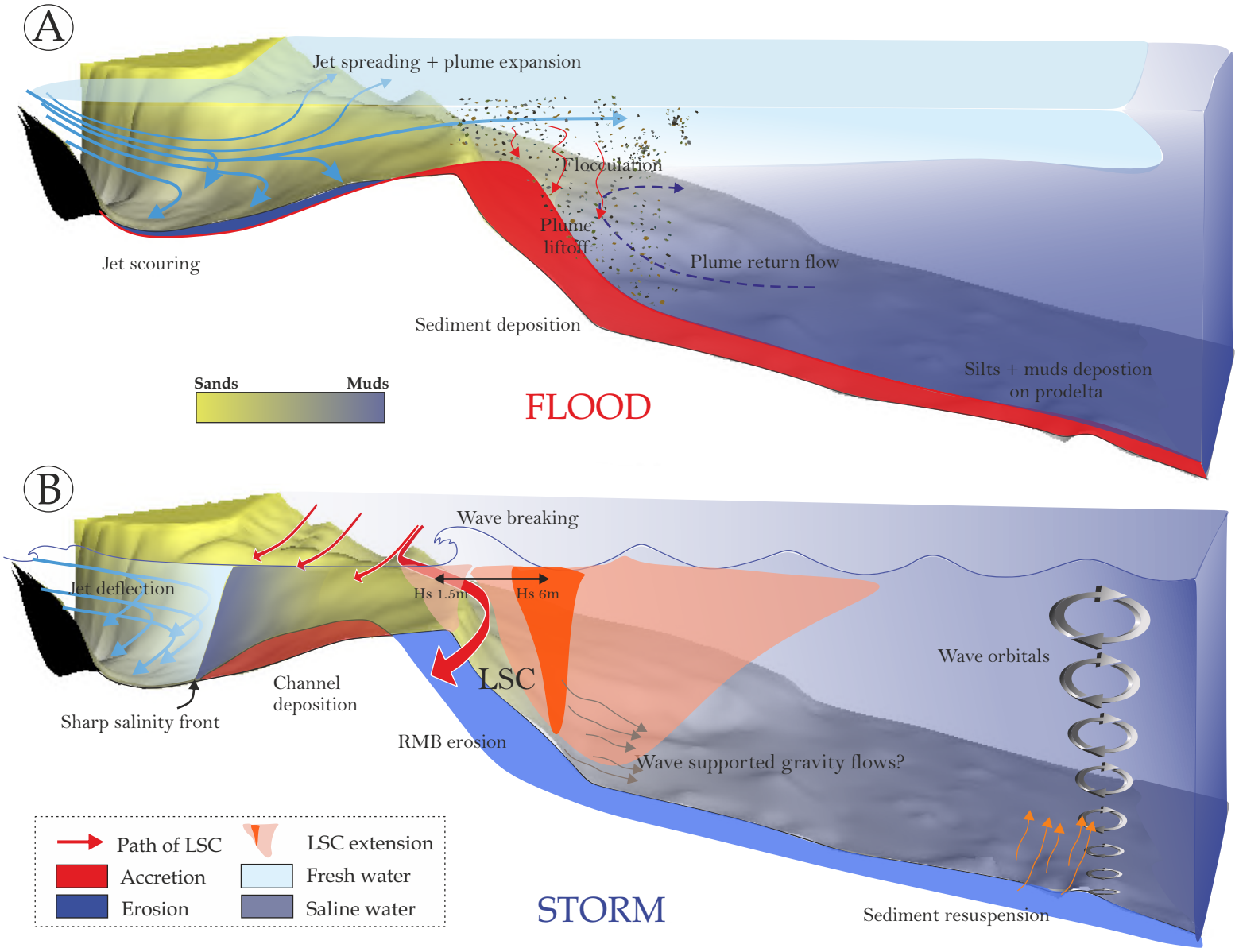
A
Jet spreading + plume expansion
Flocculation
Plume liftoff
Plume return flow
Jet scouring
Sediment deposition
Silts + muds depostion on prodelta
Sands
Muds
FLOOD
B
Wave breaking
Jet deflection
Hs 1.5m
Hs 6m
Wave orbitals
LSC
Channel deposition
Sharp salinity front
RMB erosion
Wave supported gravity flows?
Path of LSC
LSC extension
Accretion
Fresh water
Erosion
Saline water
STORM
Sediment resuspension

Discharge thresholds (m^3/s)		Wave height thresholds (m)	
Q_{15}	1000	Hs_{90}	1.5
Q_{75}	2200	Hs_{98}	2.5
Q_{95}	3200	$Hs_{99.9}$	4
$Q_{99.7}$	4000	$Hs_{99.99}$	6

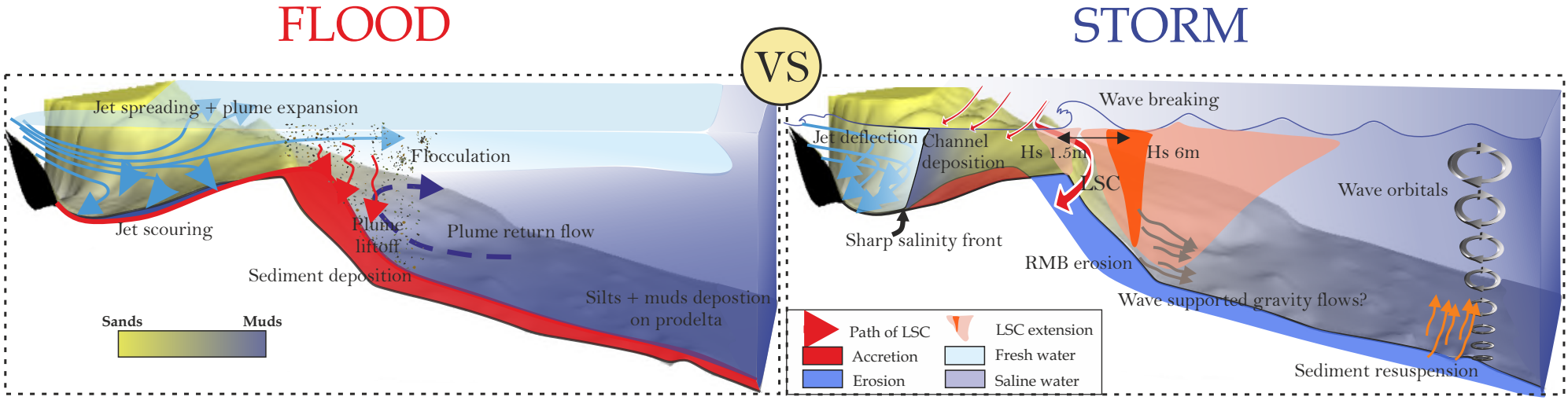
FLOOD
VS
STORM
Jet spreading + plume expansion
Flocculation
Jet scouring
Plume liftoff
Plume return flow
Sediment deposition
Silts + muds depostion on prodelta
Sands
Muds
Wave breaking
Jet deflection
Channel deposition
Hs 1.5m
Hs 6m
LSC
Wave orbitals
Sharp salinity front
RMB erosion
Wave supported gravity flows?
Sediment resuspension
Path of LSC
Accretion
Erosion
LSC extension
Fresh water
Saline water